



BACCHUS

Impact of Biogenic versus Anthropogenic emissions on Clouds and Climate: towards a Holistic UnderStanding

Collaborative Project

SEVENTH FRAMEWORK PROGRAMME
ENV.2013.6.1-2

Atmospheric processes, eco-systems and climate change

Grant agreement no: 603445

Deliverable number:	D2.4
Deliverable name:	Parameterisations for CCN and IN as a function of aerosol components, accounting for organic aerosol impact, tested in large scale models
WP number:	2
Delivery date:	Project month 36 (30/11/2016)
Actual date of submission:	01/12/2016
Dissemination level:	PU
Lead beneficiary:	ETHZ
Responsible scientist/administrator:	Ken Carslaw, Ulrike Lohmann
Estimated effort (PM):	59
Contributor(s):	Yvonne Boose, Berko Sierau (ETHZ), Ken Carslaw, Hamish Gordon, Jesus Vergara Temprado, Ben Murray (ULEEDS), Colin O'Dowd, Jurgita Ovadnevaite (NUIG), Kirsten Fossum, Christina McCluskey, Thomas C. J. Hill, Jake P. Zragoza, Paul DeMott (CSU), Matteo Rinaldi (CNR-ISAC), Ghislain Motos, Martin Gysel, Julia Schmale (PSI), Maria Kanakidou, George Fanourgakis, Stelios Myriokefalitakis (UOC), Matteo Rinaldi, Franco Belosi (CNR-ISAC)

Estimated effort contributor(s) (PM):	ETHZ: 3.5 PM, PSI: 12.5 PM, ULEEDS: 11 PM, UOC: 10 PM, NUIG: 10 PM, CSU: 8PM, CNR-ISAC: 4 PM, KIT: 0 PM
Internal reviewer:	Maria Kanakidou

Executive summary

This deliverable aims to develop and test parameterisations for cloud condensation nuclei (CCN) and ice nucleating particles (INP) as a function of aerosol components accounting for organic aerosol impact and test them in large scale models, providing input to WP3 and WP4. This includes a physically-based parameterisation of CCN activation in the presence of semi-volatile organic carbon co-condensation to implement in a variety of models and an INP parameterisation based on field measurements, remote sensing and laboratory studies. The INP data from WP1 have been the basis for the development of a parameterisation for use in a global model. In order to take the chemical properties of the INP into account, the parameterisation is based on laboratory studies of different types of aerosols and, in particular, mineral dust and biological material. The model results are evaluated against the field measurements of INP. Combined field measurements, remote sensing and biological/plankton laboratory studies and observations at Mace Head are used to develop CCN and INP parameterisations. These parameterisations are to be included in the BACCHUS ESMs.

The highlights of the results are:

- The hygroscopicity of the organic component of aerosol particles is relatively unimportant when considered alongside twenty-seven other sources of uncertainty in CCN concentration in a global aerosol microphysics model. The ability of the organic compounds to take up water is much more important for the direct radiative effect (ERF_{ari}), and is one of the major sources of uncertainty in ERF_{ari} (locally 25% of model variance) in regions with strong natural organic sources, such as forest regions.
- Over remote Southern Ocean regions the organic composition of particles plays an important role in CCN activation, but sub-dominant to the importance of the particle size distribution and number concentration.
- Models diverge with regard to the observed CCN levels and variability. The use of hygroscopicity parameters derived from field observations in BACCHUS, updated emission inventory and simultaneous representation of the INP in the models are being analysed with regard to their potential to improve the simulations of CCN.
- Primary marine organic material is a globally important ice nucleating particle (INP) component. New model simulations show that although on a monthly mean basis INPs from deserts far outnumber INP from sea spray throughout much of the low and mid-latitudes, marine organics become more important in the world's remote oceans. Furthermore, even over the northern hemisphere, marine organic INP concentrations exceed K-feldspar INP concentrations on 10-30% of the days when the temperature is within the mixed-phase range and the total concentration of INP is larger than $10^{-4} L^{-1}$. In the Southern Hemisphere, both on a monthly mean basis and on the large majority of days, marine organic aerosols are the dominant INP type from March-November.
- New measurements of INP in a coastal environment (Mace Head Observatory (53.33°N, 9.9°W) show that highest concentrations at -15°C were often associated with elevated organics and two specific events indicate important contributions of marine and terrestrial organic aerosol to the total INP

population. Nearly all INPs measured during the marine organic aerosol plume were biological in nature.

- The ice nucleation temperature of natural desert dusts varies by up to 10 K. To more adequately describe immersion freezing by desert dust in the atmosphere, mineralogy sensitive emission and transport schemes would be desirable. K-feldspar seems to be the most important INP for temperatures above 250 K. At lower temperatures Na-plagioclase feldspars and quartz emissions and transport need to be quantified in order to understand INP activity.

Contents

Executive summary	2
Contents.....	3
Summary of results.....	4
1. Parameterizations of CCN as a function of aerosol components	4
1.1. Experimental studies	4
1.1.1. PEGASO cruise (Southern Ocean)	6
1.2. CCN Modeling studies.....	10
1.2.1. Representation of CCN in large scale models.	10
1.2.2. Effects of organic compound hygroscopicity on CCN and Aerosol Optical Depth	12
1.2.3. Comparison of BACCHUS model CCN simulations with observations	15
2. Parameterizations of INP as a function of aerosol components	19
2.1. INP field experiments	19
2.1.1. BACCHUS campaign at Mace Head (North East Atlantic)	19
2.2. INP laboratory experiments	22
2.3. Global INP modelling studies.....	23
3. Reference list.....	28
Peer-reviewed publications issued from the project (BACCHUS papers).....	31
Presentations at Conferences issued from the project (BACCHUS papers)	32

Summary of results

1. Parameterizations of CCN as a function of aerosol components

1.1. Experimental studies

In BACCHUS, Schmale et al. (2016) have compiled available aerosol composition and CCN data from the ACTRIS stations and a few additional stations over the globe (Figure 1a). These data have been analyzed to achieve CCN closure (see also deliverable D2.2). This exercise enabled the evaluation of a set of aerosol component specific hygroscopicity (κ) values suitable to reproduce the observed mixed aerosol hygroscopicity. The Schmale et al. (2016) dataset is being used for the evaluation of the CCN simulations of BACCHUS projects.

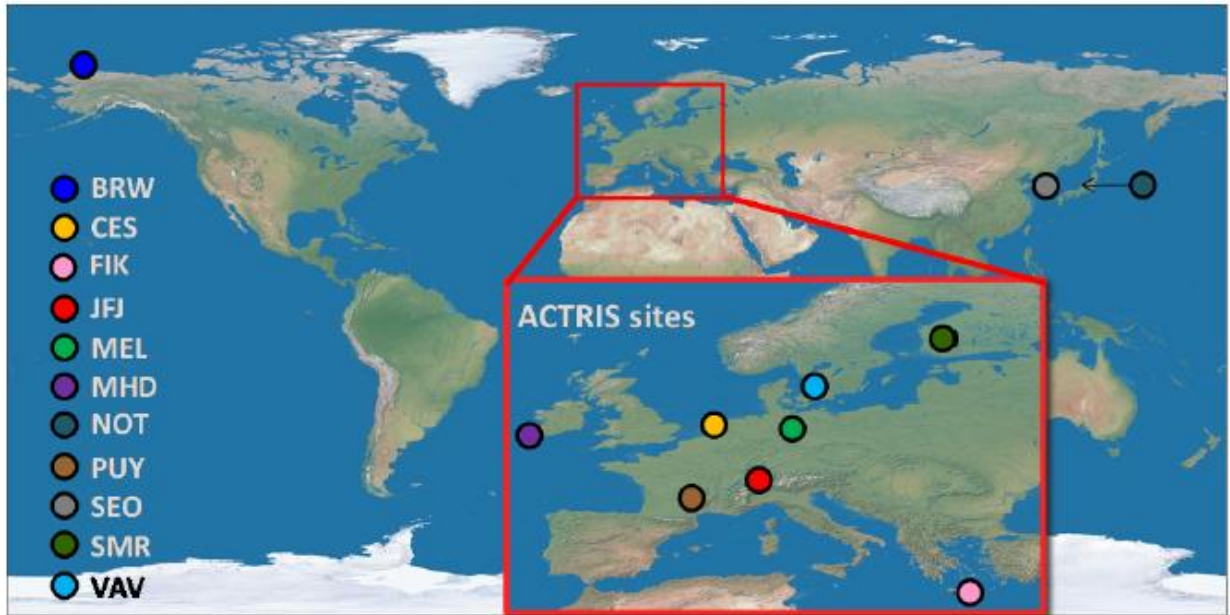


Figure 1a. Location of stations compiled by Schmale et al (2016) and used as basis for model evaluation in BACCHUS WP2.

The hygroscopicity parameter kappa (κ) quantifies the Raoult-effect, i.e. the relationship between the particle's growth factor (GF) and corresponding equilibrium relative humidity (RH). When assuming a surface tension, the κ -value unambiguously relates the dry particle size with the critical supersaturation (Petters and Kreidenweis, 2007): the higher the value of κ , the higher the hygroscopicity of a particle. The κ -value of a mixed particle can be derived from the particle chemical composition following a simple mixing rule as given in Eq. (1) when the κ -value of each component i (κ_i) is known (Petters and Kreidenweis, 2007):

$$\kappa = \sum_i \varepsilon_i \kappa_i \quad (1)$$

with ε_i being the volume fraction of component i . Volume fractions of each component were derived from their measured mass concentrations and densities (1.4 g cm^{-3} for organic aerosol).

The κ -values of pure substances typically depend on water activity. Petters and Kreidenweis (2007) provide κ -values for a variety of chemical components including inorganic salts and acids which, however, do not necessarily refer to conditions at the point of particle activation. Schmale et al. (2016) therefore calculated the pure component κ -values for a reference water activity of $a_w=0.9975$, which corresponds to the water activity at the point of CCN activation for a supersaturation of 0.5%, and a surface tension of 74.95 mN m^{-1}

(corresponding to a temperature of 5 °C as a proxy for ambient CCN activation in clouds) and, consequently, a dry particle diameter of 63.1 nm. Note that the temperature has only a minimal effect on the κ -value of a pure component. This reference water activity was used as input to the E-AIM model II (<http://www.aim.env.uea.ac.uk/aim/model2/model2a.php>) where the particulate water content was calculated for the pure salts and acids as mentioned above. Based on this, the G Fs and from that the κ -values were calculated for sulfuric acid, ammonium sulfate, ammonium bisulfate, ammonium nitrate and sodium chloride, accounting for the solution density, which is provided by the AIM model. Results (shown in Figure) are generally similar to and slightly lower than the ideal κ ($a_w=1$), but can be larger or smaller compared to the values provided in Petters and Kreidenweis (2007).

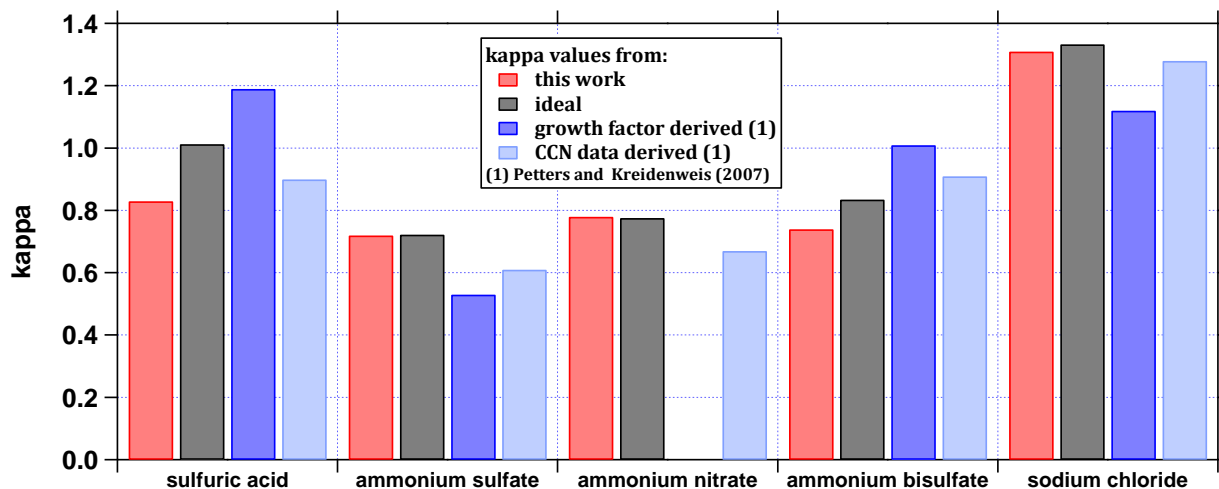


Figure 1b: Comparison of κ -values (κ_{mean}) provided in Table 1 in Petters and Kreidenweis (2007) with the new κ -values derived in this work based on a water activity of 0.9975 at the point of CCN activation as input to the E-AIM model II (<http://www.aim.env.uea.ac.uk/aim/model2/model2a.php>). The water activity was derived from the following assumptions: $\kappa = 0.3$, $SS = 0.5\%$ and $\sigma = 72.86 \text{ mN m}^{-1}$. The ideal κ -values refer to a water activity of 1.

For particulate organics, we use a κ -value of 0.1 following observations in a variety of environments (e.g. Dusek et al., 2010; Gunthe et al., 2009; Gunthe et al., 2011; Juranyi et al., 2009; Rose et al., 2011; Rose et al., 2010). It should be noted though that κ_{org} has been observed to be higher in other studies especially when the organic aerosol becomes more oxygenated (e.g., Chang et al., 2010; Massoli et al., 2010). For black carbon (BC) we use 0 (e.g., Hittenberger et al., 2003; Rose et al., 2011; Tritscher et al., 2011).

With these κ -values for individual components, we calculate the bulk aerosol hygroscopicity in five variations:

1. κ_1 : with all salts and acids as derived from the ammonium, nitrate, sulfate and chloride ions from the aerosol chemical composition data, organics, and no BC;
2. κ_2 : only with ion-balanced inorganic components which excludes acids and bisulfates, organics, and no BC;
3. κ_3 : like 1 but with BC;
4. κ_4 : like 2 but with BC;
5. κ_5 : $\kappa = 0.3$.

For stations, where no BC time series were available, seasonal or yearly average values were taken from the literature. For ATT BC concentrations were obtained from Fig. 30 in Andreae et al. (2015), for CES from Schlag et al. (2016), for SMR from Hyvärinen et al. (2011), and for FIK from (Bougiatioti et al., 2014). Results for all κ -values are provided in Table 1 below.

In addition to the κ -value, and more importantly, the size of a particle determines its ability to act as CCN. Hence, for all stations where particle number size distribution and chemical composition data are available, we can predict the number of CCN particles at a given supersaturation (SS) independently from the

observations with the CCN counter following the κ -Köhler equation (Eq. 2, Petters and Kreidenweis, 2007). This equation describes the equilibrium saturation ratio S (ratio of the partial vapor pressure of water and the saturation vapor pressure of water) over an aqueous solution droplet.

$$S = \left(1 + \kappa \frac{D_0^3}{D_{drop}^3 - D_0^3} \right)^{-1} \exp \left(\frac{4\sigma_{sol}\vartheta_w}{RTD_{drop}} \right) \quad (2)$$

with D_0 being the dry particle diameter, D_{drop} the droplet diameter, σ_{sol} the surface tension of the solution (we use a surface tension of water of 72.86 mN m⁻¹ corresponding to 20 °C which is close to the sample air temperature in the CCNC), ϑ_w the partial molar volume of water (which was assumed to be the molar volume of water) in the solution, R the universal gas constant, and T the temperature. The first term of the equation is a semi-empirical formulation for the water activity a_w . More details are given elsewhere (e.g. Jurányi et al., 2010; Petters and Kreidenweis, 2007). The maximum of Eq. 2 describes the critical supersaturation for a particle with known properties including D_0 , σ_{sol} and κ , whereby D_{drop} is the independent variable. The relationship between supersaturation and corresponding critical dry diameter (D_{crit}) for given σ_{sol} and κ has been obtained with numerical methods (see section 1.2.1).

Table 1: Median values (based on all data) for the bulk aerosol hygroscopicity parameter kappa (κ) at each station with particle chemical composition measurements. Kappa 1-5 mean: (1) includes all salts and acids as derived from the aerosol chemical composition measurements, organics, but no BC; (2) includes only ion balanced inorganic species, organics and not BC; (3) like (1) but with BC; (4) like 2 but with BC; (5) $\kappa = 0.3$.

Station	κ 1	κ 2	κ 3	κ 4	κ 5
ATT	0.26	0.21	0.25	0.20	0.30
CES	0.52	0.50	0.50	0.48	0.30
FIN	0.46	0.47	0.46	0.45	0.30
JFJ	0.41	0.31	0.39	0.29	0.30
MEL	0.43	0.42	0.42	0.42	0.30
MHD	0.63	0.63	0.61	0.61	0.30
SMR	0.30	0.29	0.27	0.25	0.30

Having determined D_{crit} at a given SS we can calculate the number of activated particles by integrating the particle number size distribution from its maximum diameter (D_{max}) down to D_{crit} following Eq. 3:

$$N_{CCN}(SS) = - \int_{D_{max}}^{D_{crit}(SS)} \frac{dN(D)}{d \log D} d \log D \quad (3)$$

$N_{CCN}(SS)$ can then be compared to the measured number of CCN at the same SS by the CCN counter.

1.1.1. PEGASO cruise (Southern Ocean)

The PEGASO (Plankton-derived Emissions of trace Gases and Aerosols in the Southern Ocean) cruise was conducted on board de RV Hesperides in the regions of Antarctic Peninsula, South Orkney and South Georgia Islands from 2 January to 11 February 2015. A dependence of CCN activation on aerosol chemical composition as well as the origin of air masses was investigated. It is well known that CCN activation can be significantly affected by the high organic fraction in a marine environment (O'Dowd et al., 2004). Moreover, it has been shown that while organics found in polluted environments shows hydrophobic properties, marine organics

are dichotomously water repellent while retaining relatively high CCN activation efficiencies (Ovadnevaite et al., 2011). Therefore, particular attention was paid to the CCN-organic matter relationship in the Southern Ocean.

The size resolved non-refractory chemical composition of submicron aerosol particles was measured with an Aerodyne High Resolution Time of Flight Aerosol Mass Spectrometer (DeCarlo et al., 2006). Aerosol size distributions were measured by a TSI scanning mobility particle sizer (SMPS) and a relative humidity <40%. CCN concentrations were determined by a Droplet Measurements Technology CCN counter (Lance et al., 2006), operated in size segregated mode. Aerosol GFs were measured using a Hygroscopic Tandem Differential Mobility Analyzer (HTDMA) that followed the EUSAAR standard installation and accuracy. GFs at 90% RH were determined for dry size particles of 35, 50, 75, 110 and 165 nm. Black carbon concentrations were derived from SP2. 72 hour air mass back-trajectories were obtained from HYSPLIT model (Stein et al., 2015) at 100 m over the ships location at time. Chl-a daily averages were obtained via satellite imaging averaging for 0.1° x 0.1° resolution.

Steady-state air mass periods were selected for this study to derive typical aerosol properties for different Southern Ocean regions. To fulfill this criterion, an air mass had to remain stable for more than 4 hrs. E.g. particle size distributions had to be constant (deviations < 20% of total particle number and size) for the whole period, as well as the chemical composition, in addition to stable meteorological conditions. Moreover, the air mass source region had to remain unchanged relative to the ship's movement. Twelve periods were found that satisfied these conditions corresponding to four different source region types. Figure 2 shows all 4 regions: Weddell Sea (W), South Atlantic (SA) air mass, Southern Ocean (SO) air mass and the fourth being a mixture of two or more.

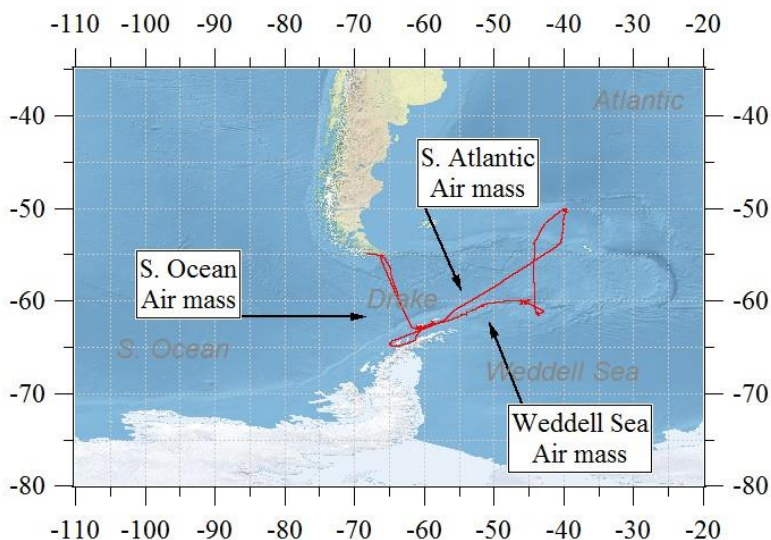


Figure 2. Map of main air mass source regions. PEGASO cruise ship path is marked in red.

CCN properties were dependent on the region where aerosol particles were originated. The critical activation diameters derived from size segregated CCN measurements at different supersaturations for all stable cases found for the cruise are shown in Figure 3. Letters beside the case numbers indicate the source region of the period. The relationships of CCN critical diameter with supersaturation for different cases indicate that while aerosol in Weddell Sea air masses had lower or similar CCN activity to ammonium sulphate (AS), aerosol in S. Ocean air masses acted like AS for smaller particle sizes (higher supersaturations), but tended towards the better NaCl activation efficiency at larger particle sizes (lower supersaturations). This behaviour points to externally mixed sea salt and nss-sulphate (nss-SO₄) particles. It was consistent with the chemical composition

measured for different periods. Weddell cases were dominated by nss-SO_4 , making up a fraction of more than 60% of the chemical composition. In contrary, the S. Ocean cases were notably different in their chemical composition with dominant sea salt contribution followed by OM and sulphate. On average, CCN slopes indicated better activation (smaller dry critical diameter at certain supersaturation) for cases related to S. Ocean or S. Atlantic regions with the most active slope observed for the Case 7, which corresponded to the air mass originated from the S. Ocean with high wind speeds, and chemically dominated by sea salt particles and organics. At the same time, Weddell Sea cases, on average, were less active or required larger critical diameters.

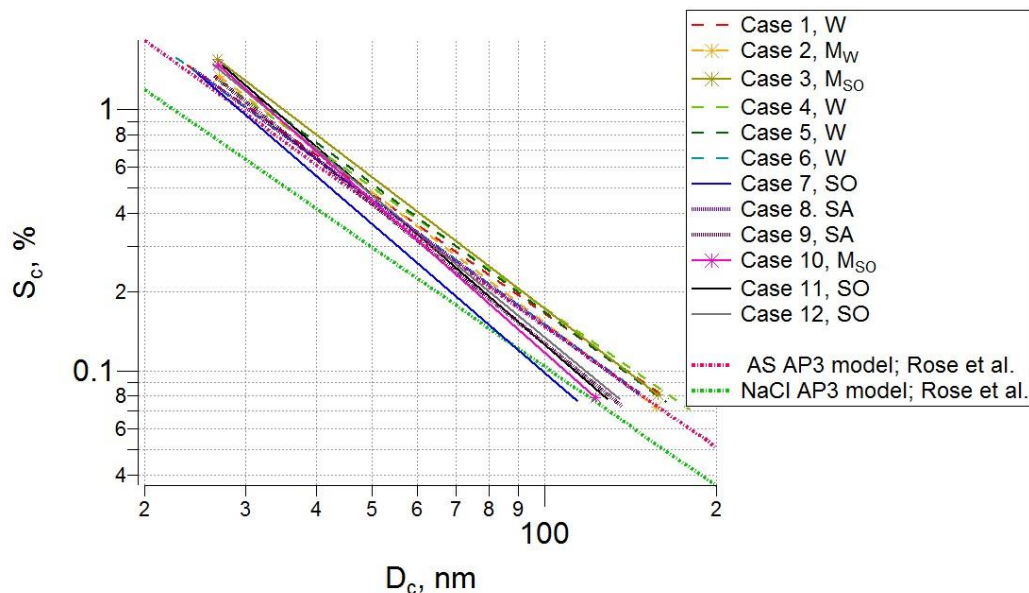


Figure 3. Critical supersaturations for critical diameters obtained from the CCNC set-up. Each case is shown as well as two sets of data taken as the standard for AS ($(\text{NH}_4)_2\text{SO}_4$), and NaCl. The following are the source region for each abbreviation in the key: W, Weddell Sea; SO, S. Ocean; SA, S. Atlantic; M_W , mixed source region dominated by Weddell Sea; M_{SO} , mixed source region dominated by S. Ocean.

On the other hand, the ratios of CCN to total number concentration (above 20nm) depict a higher fraction of activated particles for Weddell Sea cases if compared to S. Ocean cases (Figure 4). This ratio hugely depended on the real particle size distributions observed in the individual regions. S. Ocean cases showed consistently smaller particle diameters than aerosol distributions from other regions. The effect of size distribution on CCN concentration can be illustrated by Southern Atlantic Ocean case 8 that showed notably higher fraction of CCN activation due to its mono-modal aerosol distribution with particle mode diameters ranging from 60 to 100 nm. Due to this size distribution and CCN activation curve similarity to AS activation, almost all particles were activated at supersaturations higher than 0.6%.

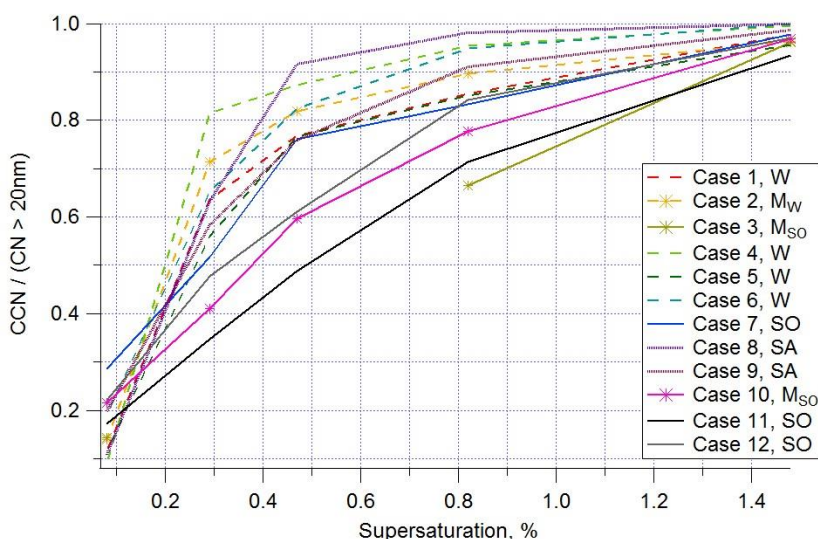


Figure 4. Above: Ratio of CCN number derived from critical diameters to all particles greater than 20 nm. Abbreviation in the key: W, Weddell Sea; SO, S. Ocean; SA, S. Atlantic; Mw, mixed source region dominated by Weddell Sea; Mso, mixed source region dominated by S. Ocean.

Nonetheless, CCN concentrations were dependent on aerosol chemical composition and correlated with Chl-a concentration (Table 2). Correlation coefficient between CCN and organic mass concentration reached up to 0.93 at 0.47% supersaturation indicating strong CCN dependence on OM concentration. Also, CCN correlated well with nss-SO₄ concentration, though slightly worse than OM and correlation coefficient reached 0.83 at 0.29% supersaturation. There was a statistically significant correlation (0.76) between CCN and organic nitrogen, but not with methanesulfonic acid (MSA). As mentioned above, CCN concentrations correlated with Chl-a and the correlation coefficient was equal to 0.57 (p=0.05), which is still significant but not as strong as for OM or nss-SO₄, which points to a more complicated relationship between CCN concentration and biological activity in the Southern Ocean.

Table 2. Correlation coefficients of CCN at different supersaturations and aerosol chemical composition, as well as Chl-a for 12 stable cases. Red numbers represent significance with p=0.01 and blue p=0.05.

Correlation Table, R-values	Chl-a	OM	Nitrate	nss-SO ₄	Ammonium	MSA	ON	Sea Salt	CCN at 1.48%	CCN at 0.82%	CCN at 0.47%	CCN at 0.29%	CCN at 0.08%
Chl-a	1.00	0.59	0.73	0.47	0.51	0.13	0.64	-0.28	0.45	0.51	0.57	0.57	0.10
OM	0.59	1.00	0.23	0.62	0.67	0.29	0.85	-0.21	0.82	0.88	0.93	0.91	0.42
Nitrate	0.73	0.23	1.00	0.48	0.52	0.35	0.40	0.05	0.33	0.32	0.30	0.28	0.21
nss-SO ₄	0.47	0.62	0.48	1.00	0.83	0.71	0.68	-0.17	0.80	0.82	0.80	0.83	0.61
Ammonium	0.51	0.67	0.52	0.83	1.00	0.56	0.78	0.00	0.76	0.78	0.76	0.76	0.57
MSA	0.13	0.29	0.35	0.71	0.56	1.00	0.42	-0.14	0.45	0.42	0.43	0.45	0.34
ON	0.64	0.85	0.40	0.68	0.78	0.42	1.00	-0.31	0.63	0.71	0.76	0.76	0.27
Sea Salt	-0.28	-0.21	0.05	-0.17	0.00	-0.14	-0.31	1.00	0.19	0.06	-0.09	-0.13	0.57
CCN at 1.48%	0.45	0.82	0.33	0.80	0.76	0.45	0.63	0.19	1.00	0.99	0.95	0.94	0.80
CCN at 0.82%	0.51	0.88	0.32	0.82	0.78	0.42	0.71	0.06	0.99	1.00	0.99	0.98	0.74
CCN at 0.47%	0.57	0.93	0.30	0.80	0.76	0.43	0.76	-0.09	0.95	0.99	1.00	1.00	0.62
CCN at 0.29%	0.57	0.91	0.28	0.83	0.76	0.45	0.76	-0.13	0.94	0.98	1.00	1.00	0.60
CCN at 0.08%	0.10	0.42	0.21	0.61	0.57	0.34	0.27	0.57	0.80	0.74	0.62	0.60	1.00

In summary, CCN activation efficiency was mostly controlled by the chemical aerosol composition, but the total CCN number concentrations depended on the aerosol particle number concentration and the size distribution. On average, Weddell Sea influenced aerosol cases possessed higher CCN ratio to total particle concentration, but mainly due to its larger aerosol sizes rather than the chemical composition. The CCN and Chl-a relationship points to a potential of using Chl-a as a proxy for biological activity in the ocean and resulting CCN activation, but the dependency has to be investigated more closely, possibly invoking the lag (O'Dowd

et al., 2015) between the biological productivity and resulting aerosol chemical composition as well as CCN activation.

1.2. CCN Modeling studies

1.2.1. Representation of CCN in large scale models.

The BACCHUS models are using parameterizations of various complexity and with different input parameters to simulate CCN formation. These are summarized as follows:

ECHAM6-HAM2. ECHAM6 is a global climate model (Stevens et al., 2013) coupled to the microphysical aerosol module HAM2 (Zhang et al., 2012), together with a microphysical cloud scheme (Lohmann et al., 2007; Lohmann and Hoose, 2009). The aerosol size distribution in ECHAM6-HAM2 is described by seven log-normal aerosol modes: four soluble (nucleation, Aitken, accumulation and coarse) and three insoluble modes (Aitken, accumulation and coarse). Sulfate (SU), black carbon (BC), particulate organic matter (POM), sea salt (SS) and mineral dust (DU) are the aerosol components used in the current setup (cf. Fig. 1 in Zhang et al., 2012). The aerosol components in the insoluble modes (BC, POM, DU) can be transferred to the soluble modes by condensation of sulfuric acid from the gas phase or coagulation with aerosols of the soluble modes.

Activation of CCN is described by Stier (2016). ECHAM6-HAM2 uses in the current setup an explicit Köhler theory based activation scheme with empirical estimation of maximum supersaturation in updrafts derived from explicit parcel model calculations (Abdul-Razzak and Ghan, 2000). The total number of activated particles is calculated as a sum of the integrated log-normal aerosol number distribution from the radius of activation for each mode. POM as well as DU in the soluble modes are treated as wettable and in the insoluble modes as entirely hydrophobic (Stier, 2016).

Immersion and contact freezing by DU and BC are considered for the heterogeneous freezing in mixed-phase clouds. The parameterizations are based on Lohmann and Diehl (2006). Soluble DU and BC act as immersion nuclei while insoluble DU acts as contact nuclei. DU nuclei are considered to have the freezing properties of montmorillonite (Lohmann and Hoose, 2009).

GLOMAP. In the global chemistry-transport model GLOMAP, CCN is calculated using the standard Kappa approach, where the following κ values are assumed:

$$\kappa_{\text{SO}_4} = 0.61$$

$$\kappa_{\text{OC}} = 0.1 \text{ (default)}$$

$$\kappa_{\text{NaCl}} = 1.28.$$

$$\kappa_{\text{BC}} \text{ and } \kappa_{\text{Dust}} = 0$$

CCN is currently calculated as a post-processing step (on line calculation of this model output is being implemented in the model). The post processing code takes into account the mass, size and composition of each soluble mode to calculate the fraction of the mode that would activate given a reference supersaturation. This code is written in IDL, though a Python version is also available.

In GLOMAP perturbation of κ_{OC} affects (i) the water uptake of the aerosol, and therefore the ambient aerosol size. This ambient size is used in the calculation of the aerosol optical depth, so in its current form GLOMAP does not account for a feedback from κ_{OC} to AOD. Change in κ_{OC} also affects (ii) cloud droplet number as the κ value is used in the activation calculation. So changing κ_{OC} affects cloud droplet number (CDN) (both directly

through changes in activation, and also indirectly through changes in the aerosol distribution due to different deposition, coagulation rates through the change in ambient size).

NorESM. The parametrization used for NorESM2 to calculate CCN uses the formulation of Abdul-Razzak and Ghan, 2000). This formulation counts the number of particles, which would have been activated at a certain supersaturation to become CCN. In the current formulation in NorESM, the particles, which are already inside a cloud droplet, are not considered to be CCN.

NorESM has 12 size-modes contributing to the CCN-formation. The aerosol model is documented in Kirkevåg et al. (2013). The description of secondary organic aerosol (SOA) is now based on (inspired by) Makkonen et al (2014). CCN have not been evaluated against measurements outside of BACCHUS. Aerosol concentrations have been evaluated through comparing to AEROCOM (<http://aerocom.met.no/Welcome.html>) measurements of mass concentrations and optical depths.

INP are calculated by a formulation based on Wang et al. (2014). It accounts for the cloud-borne aerosol number concentration of dust and soot in case of immersion freezing, an older version used activated particles instead. Deposition nucleation and contact freezing depend on the uncoated aerosol number of dust and soot. INP have not been compared or evaluated against observations. It has only been checked that the calculated concentrations are within reasonable ranges.

TM4-ECPL. Aerosol dynamics are parameterized in TM4-ECPL using the M7 microphysics model (Vignati et al., 2004). Atmospheric particles are divided into internally mixed water-soluble particles and insoluble particles. The time evolution of the particle sizes is described using log-normal distributions. Depending on their size, water soluble particles are found in the nucleation mode (particle diameter 1-10 nm) which contains sulfuric acid (SU), in the Aitken mode (particle diameter 10-100nm) which contains SU, black carbon (BC) and organic carbon (OC), and in the accumulation (particle diameter 100nm-1µm) and coarse modes (particle diameter > 1µm) which contain SU, BC, OC, dust (DU) and sea-salt (SS). In the model, insoluble particles are present in the insoluble Aitken mode (BC and OC), and in the insoluble accumulation and coarse modes (DU). Insoluble particles become soluble when there is sufficient amount of soluble material. The M7 describes new particles formation by nucleation, mixing and growth by condensation, and coagulation (Vignati et al., 2004). Other physical processes, such as, dry and wet deposition, are described by the TM4-ECPL model (Daskalakis et al., 2015, 2016; Myriokefalitakis et al., 2016).

The number of particles that will activate to form CCNs depends on the specific atmospheric conditions (i.e. temperature T and supersaturation S) and the chemical composition of the particles. The calculation of the critical particle-size for particle activation is based on the κ -Köhler theory as described by Petters and Kreidenweis (2007). The chemical composition of an internally mixed particle is characterized by the total hygroscopicity parameter, κ , according to the equation (1) (see 1.1.) that is a function of the volume fraction of the component i (ϵ_i), and κ_i , its corresponding hygroscopicity parameter. For a given supersaturation ratio, S , the critical dry diameter D_d for particle activation is computed by iteratively solving equation (4):

$$S(D) = \frac{D^3 - D_d^3}{D^3 - D_d^3(1-\kappa)} \exp\left(\frac{4\sigma_w/\alpha M_w}{RT\rho_w D}\right) \quad (4)$$

where R is the universal gas constant, D is the droplet diameter, and M_w , ρ_w , $\sigma_{s/a}$ are the molecular weight, density and surface tension of water, respectively. The number of CCNs is computed by analytical integration of the log-normal distributions for sizes larger than the critical one. Only water-soluble particles can act as CCN (Spracklen et al., 2011).

During the simulations with the TM4-ECPL, for the selected observation stations, masses of individual components and particle sizes for all soluble modes were stored every hour and CCN were calculated afterwards as a post-processing step. This procedure allows for a computationally efficient study of the sensitivity of CCNs to the hygroscopicity parameter, κ , of the individual components (see Deliverable 2.2 section 4.1 for such sensitivity studies performed with TM4-ECPL).

For the TM4-ECPL results presented in the next section, the hygroscopicity parameters used are: $\kappa_{\text{SU}}=0.61$, $\kappa_{\text{OC}}=0.2$, $\kappa_{\text{BC}}=0$, $\kappa_{\text{SS}}=1.28$, $\kappa_{\text{DU}}=0$. TM4-EPCL model was run with ACCMIP and RCP6 anthropogenic and biomass burning emissions in its low resolution version ($6^\circ \times 4^\circ$ longitude \times latitude) using ECMWF ERA interim meteorology (Daskalakis et al., 2016). The higher resolution simulations using CMIP6 emissions are ongoing and will be reported in D2.5.

1.2.2. Effects of organic compound hygroscopicity on CCN and Aerosol Optical Depth

ULEEDS performed a large global model sensitivity analysis to quantify the effect of organic compound hygroscopicity on CCN and AOD. A large perturbed parameter ensemble (PPE) of the HadGEM-UKCA model was created as part of a separate project in the UK (the Global Aerosol Synthesis and Science Project, GASSP). In BACCHUS we used the results to isolate the effect of organic compounds.

The PPE consisted of over 200 1-year simulations of the global model with 26 aerosol parameters sampled using a Latin hypercube approach. Emulators were built for each model grid box at the surface to define the relationship between the outputs (e.g., CCN) and the uncertain parameters across the 26-dimensional space. The uncertainty in the outputs was then calculated by Monte Carlo sampling of the emulated values. Each uncertain parameter has a probability distribution (Figure 5), which was based on expert elicitation. The resulting output uncertainty ranges and distributions therefore account for the likelihood distributions of all the parameters.

To explore the effect of uncertainty in organic compound hygroscopicity we varied κ of the organic component in the aerosols (κ_{OC}). The value of κ_{OC} is assumed to lie in the range 0.1-0.6, with the greatest likelihood to lie between about 0.15 and 0.3 (see Figure 5). The κ value is applied equally to the sum of organic carbon in the aerosol, including anthropogenic and natural sources.

CCN in the model are calculated assuming $\kappa_{\text{SO}_4} = 0.61$, $\kappa_{\text{NaCl}} = 1.28$ and $\kappa_{\text{BC/dust}} = 0$. When we perturb κ_{OC} in the model it affects the water uptake of the aerosol, and therefore the ambient aerosol size. This ambient size is used in the calculation of the aerosol optical depth, so we do have a coupling to AOD. It also affects the cloud droplet number as κ is used in the activation calculation. So changing κ_{OC} affects CDN (both directly through changes in activation, and also indirectly through changes in the aerosol distribution due to different deposition, coagulation rates through the change in ambient size).

By sampling from the multi-dimensional emulators it is possible to extract the fraction of CCN or AOD variance caused by the assumed uncertainty in κ_{OC} (Figures 6 and 7). Our results show that κ_{OC} contributes locally about 2-5% of the CCN variance as an annual mean. We also show results for July when κ_{OC} uncertainty has its largest effect and compare the effect to the overall uncertainty in CCN from sampling all parameters. The largest absolute effect on CCN occurs, as expected, over regions with large organic emissions, particularly over the boreal forest, West Africa and Amazonia. In contrast, the largest relative effect (relative to all other uncertainties) occurs over ocean regions. The reason for this geographical pattern is that there are larger sources of uncertainty over the land than over the ocean, so the relative effect of κ_{OC} is diminished over land, and in fact becomes negligible.

The absolute uncertainty is defined as the square root of the variance caused by the uncertainty in κ_{OC} (i.e., this is effectively the CCN ‘standard deviation’ caused by κ_{OC}), although the standard deviations of the individual parameters cannot be combined to estimate the total standard deviation. We estimate the standard deviation in CCN caused by κ_{OC} to be approximately $10\text{-}15\text{ cm}^{-3}$ over the main natural emission regions. Our results therefore suggest that uncertainty in κ_{OC} (as defined by the probability distribution in Fig 5) is negligible compared to other uncertainties in the model.

We also investigated the effect of the κ_{OC} on the AOD and direct radiative forcing over the industrial period. Here we find much larger effects, with the fraction of AOD and ERF_{ari} variance as high as 25% over strong biogenic emission regions. We therefore conclude that the uncertainty κ_{OC} is much more important for the aerosol radiative effects than it is for CCN.

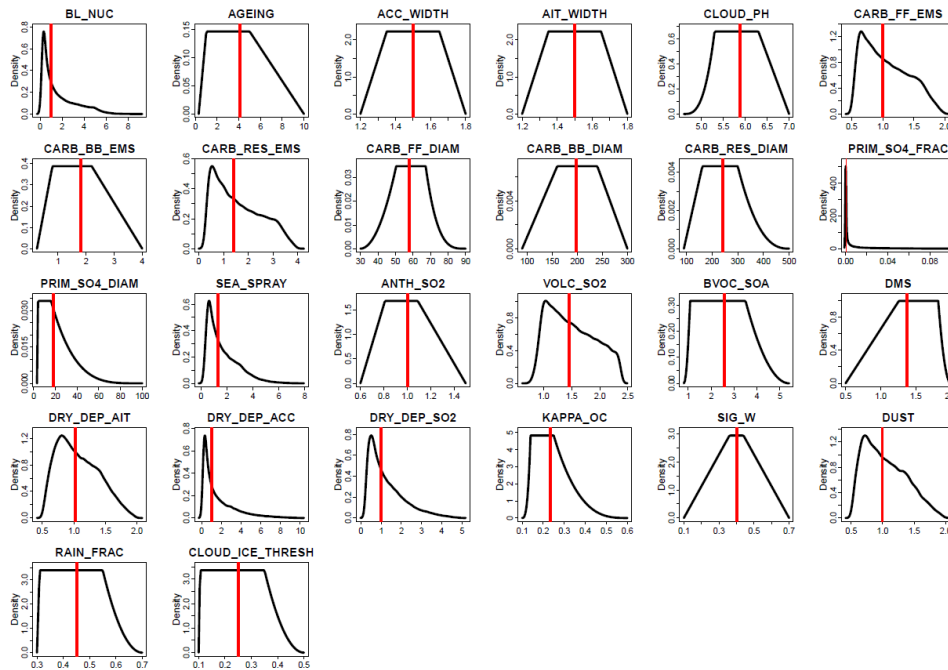


Figure 5. Probability distributions of uncertain model parameters sampled in the HadGEM-UKCA perturbed parameter ensemble.

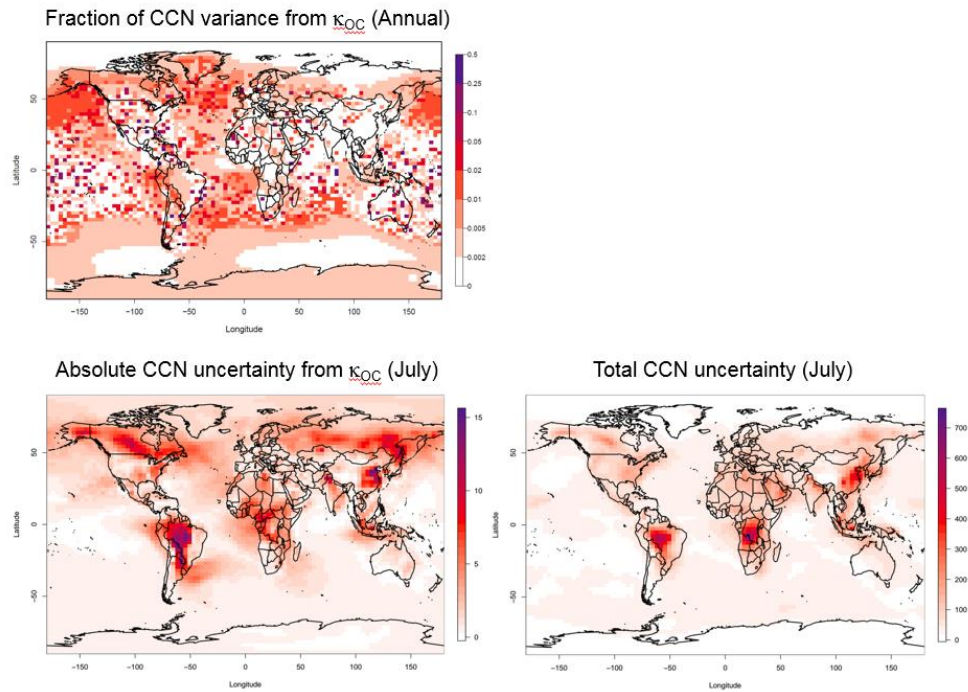


Figure 6. Uncertainty in CCN at 0.2% supersaturation caused by uncertainty in κ_{OC} . Top left: Fraction of total CCN variance (from all parameter perturbations) caused by the assumed uncertainty in κ_{OC} in Fig 5. Bottom left: absolute uncertainty in CCN in July. Bottom right: total uncertainty from all parameters in July for comparison (different scale).

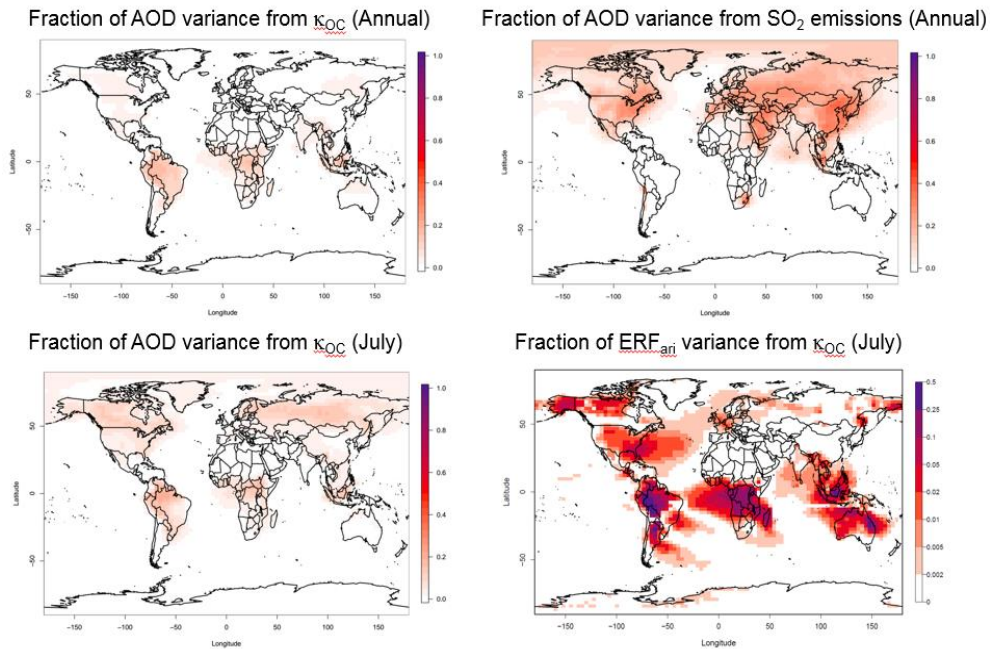


Figure 7. Uncertainty in aerosol optical depth (AOD at 550 nm) and ERF_{ari} over the industrial period caused by uncertainty in κ_{OC} . Top left: Fraction of AOD variance caused by κ_{OC} . Top right: Fraction variance in CCN caused by uncertain anthropogenic SO_2 emissions (for comparison). Bottom left: Fraction of AOD variance in July. Bottom right: Fraction of ERF_{ari} variance.

1.2.3. Comparison of BACCHUS model CCN simulations with observations

In order to evaluate the uncertainties in the computed CCN concentrations issued from the model parametrizations a BACCHUS model intercomparison exercise has been initiated in WP2 with the set up that has been described in the Deliverable 2.2 and the first output of the models were due end of November 2016. Here some first results are shown while a thorough comparison will be provided in Deliverable 2.5 and will be the subject of a research article.

Currently only NorESM and TM4-ECPL preliminary hourly model results have been made available for this comparison presented in the following figures. As mentioned above TM4-ECPL simulation is a low resolution model (6°x4°) which needs to be updated with regard to the anthropogenic emission inventories used in the model. The updated ongoing higher resolution simulations are expected to perform better and will be reported in D2.5.

The hourly values have been averaged first on a daily basis (Figure 8), then on a monthly basis (Figure 9) and then all years for the same month have been averaged to provide the seasonal variability of CCN shown in Figure 10 for selected surface stations with available CCN and aerosol chemical composition data from Schmale et al (2016). Observational averages have been computed in a similar manner, where hourly values are available. Since measurements are in some cases quite sparse, the obtained daily and monthly averages may differ significantly from the exact ones. While the present approach for computing the various averages is exact within the model accuracy, in the future for a more accurate comparison of the model results with observations, model averages will be computed using only the hours for which observations are available. These results will be reported in deliverable 2.5.

The preliminary results show significant differences between the models as well as with the observations. In general TM4-ECPL calculates higher CCN concentrations than NorESM. One possible reason for this is that the present version of TM4-ECPL does not distinguish between CCN and INP, therefore it is expected to overestimate CCN where INP might be important. Another reason could be differences in the aerosol composition in the two models. In general both models reproduce reasonably well the distributions at Finokalia station in Crete. TM4-ECPL overestimates the levels at Hyytiälä and Jungfraujoch. The low spatial resolution of the model is expected to affect the model results. In particular, at mountain stations (like Jungfraujoch shown below) the 'mean surface level' in the corresponding large model surface grid is significantly lower than the actual height of the station. In addition due to the size of the grid, the simulated aerosol composition and concentration corresponds to a mixture with the pollution from the surrounding areas. These factors are affecting the comparison of model to observations, which at Jungfraujoch shows an overestimate of CCN levels. On the opposite NorESM computes in general low CCN concentrations, which are however relatively close to the observations at several altitude locations, in particular at Jungfraujoch and at the remote location of Finokalia, while at Cabauw and Hyytiälä it underestimates them. There TM4-ECPL is performing better than NorESM.

Day-to-day variations: As in the observations, the models reproduce a large day-to-day variability in CCN of about a factor of 3-5 that reflects differences in the meteorological conditions and the aerosol composition (Figure 8).

Monthly and interannual variations: A larger monthly and interannual variability is seen in the observed CCN at various locations than simulated by the NorESM. TM4-ECPL driven by ERA-interim meteorology, shows a higher variability than NorESM in CCN with amplitudes closer to the observed ones, although the absolute CCN values are high (Figure 9).

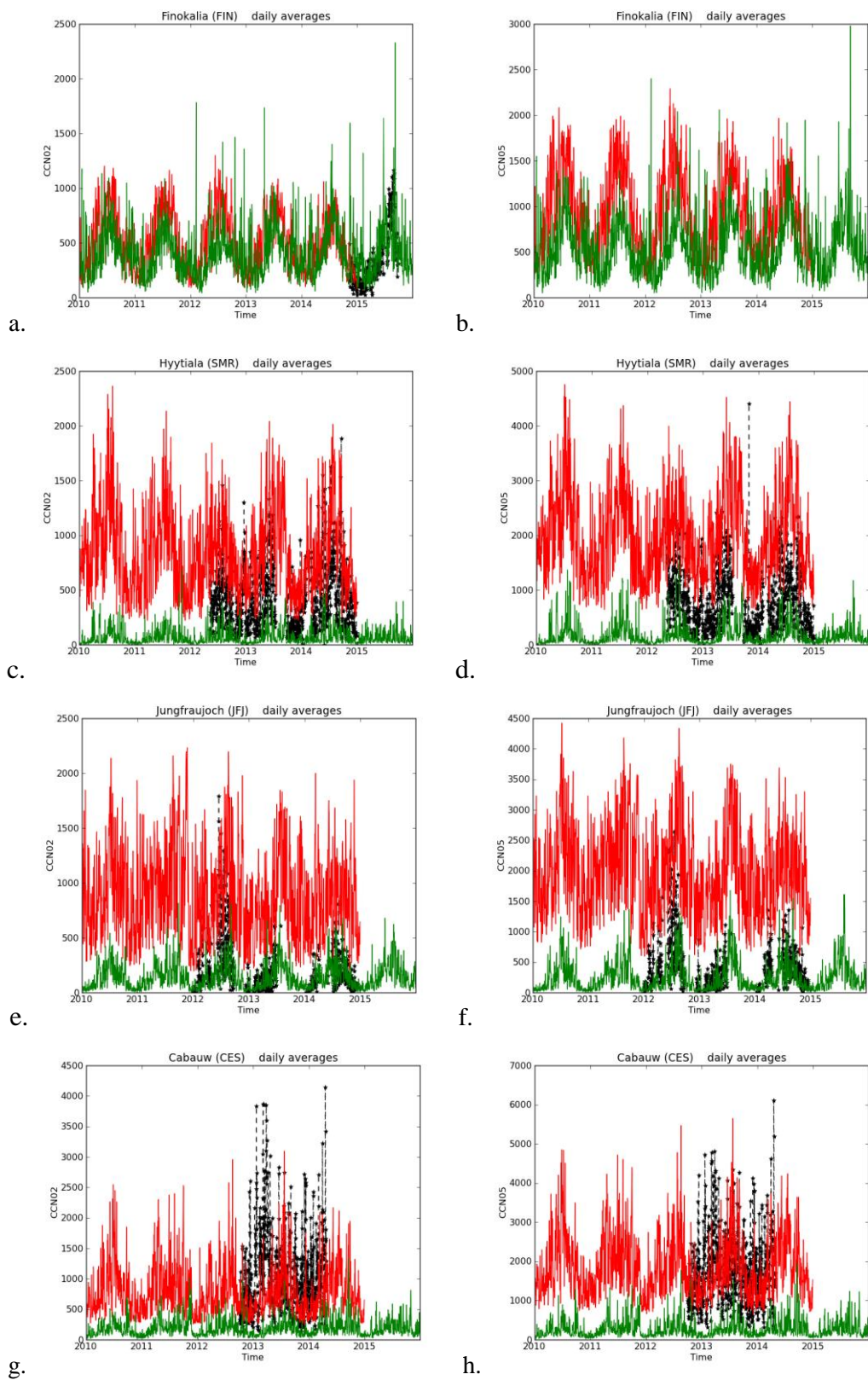


Figure 8. Daily comparisons between model results and observations of CCN at 0.2% ss (left panels) and 0.5% ss (right panels) at some of the surface stations with available data from Schmale et al. (2016) (black symbols). Models are TM4-ECPL (in red) and NorESM (in green). Units are cm^{-3} .

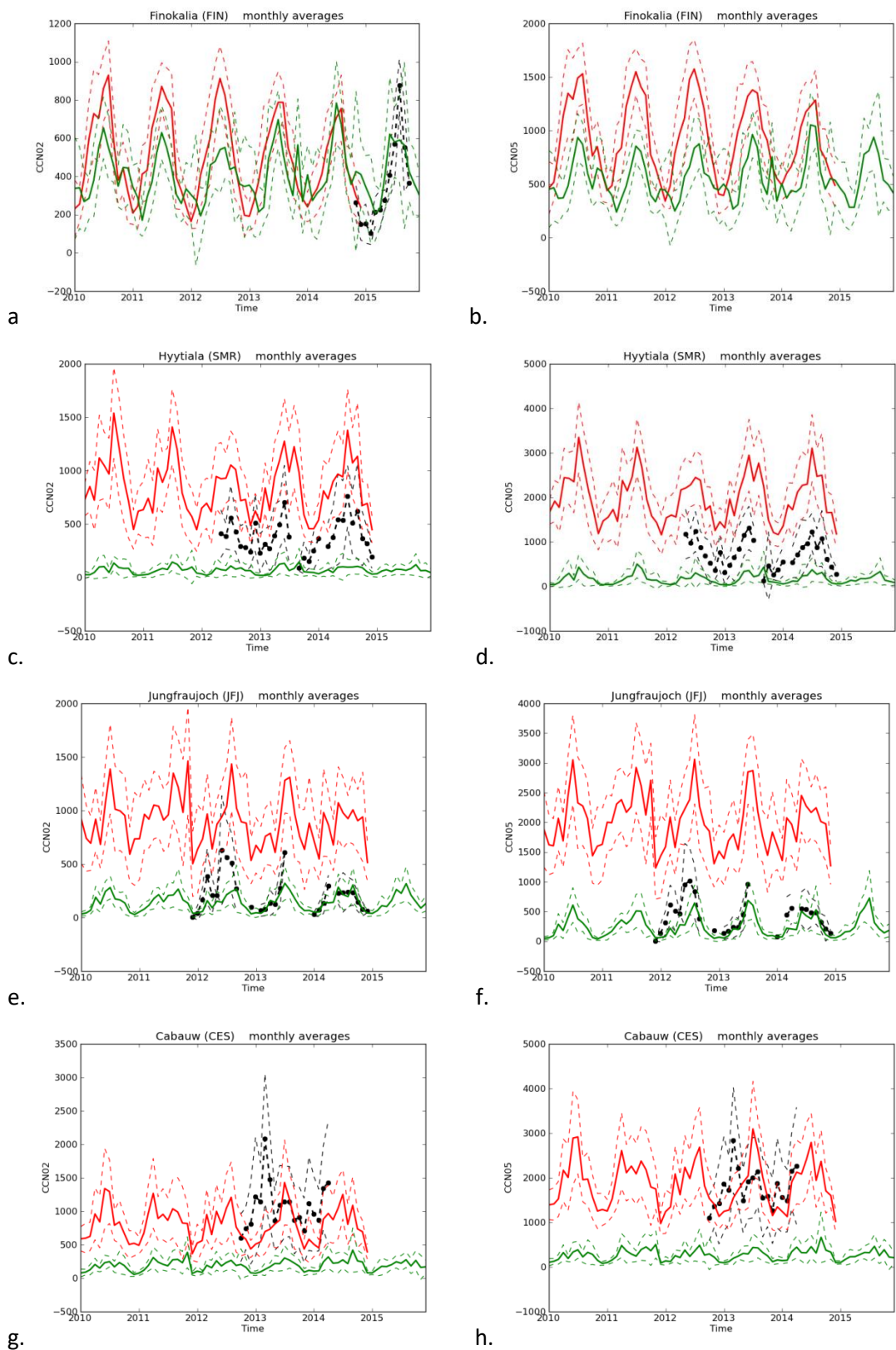


Figure 9. Monthly comparisons between model results and observations of CCN at 0.2% ss (left panels) and 0.5% ss (right panels) at some of the surface stations with available data from Schmale et al. (2016) (black symbols). Models are TM4-ECPL (in red) and NorESM (in green). Units are cm^{-3} . Dashed lines provide the width of one standard deviation of observations and model results with the respective colors.

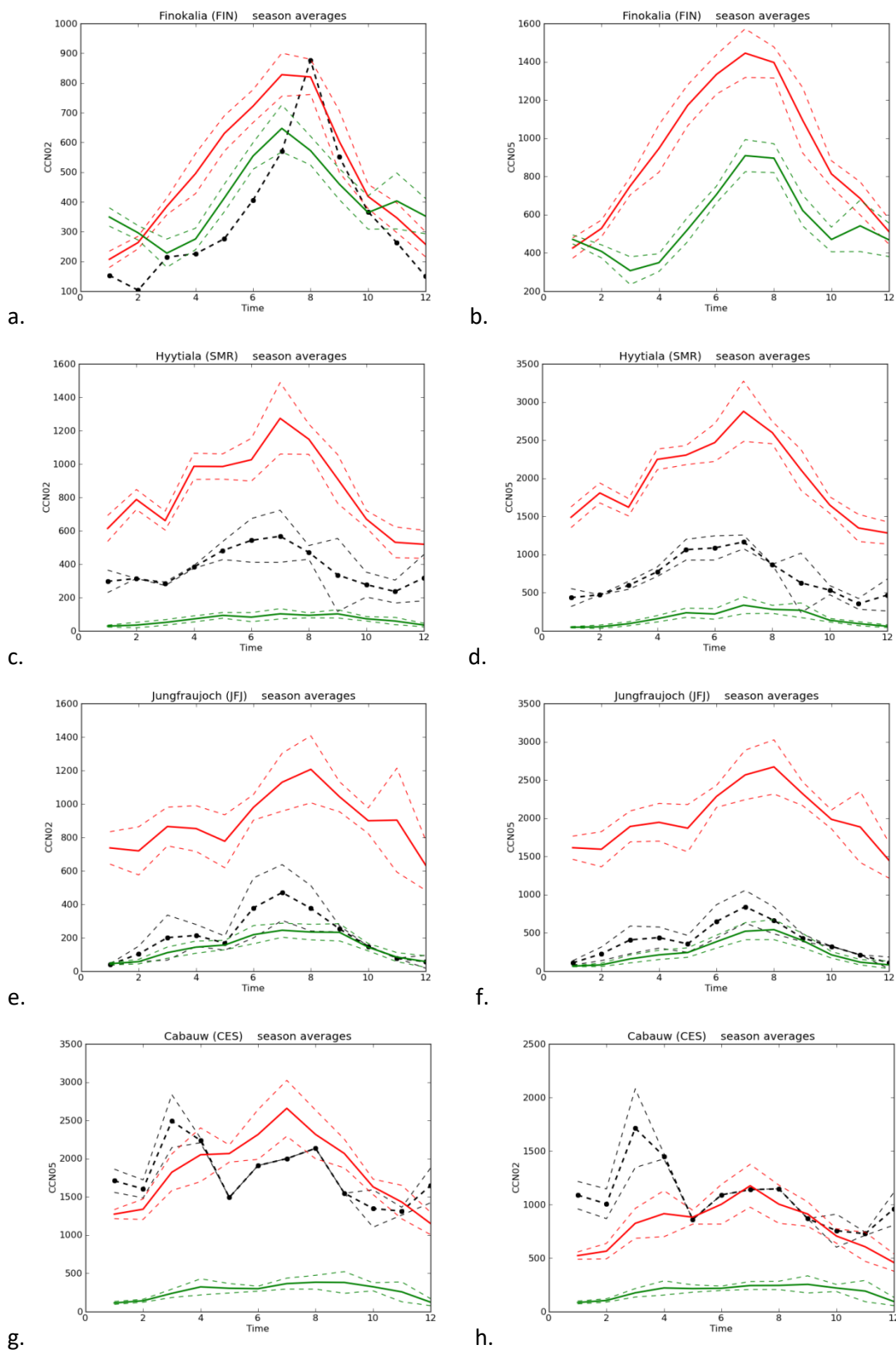


Figure 10. Seasonal comparisons between model results and observations of CCN at 0.2% ss (left panels) and 0.5% ss (right panels) at some of the surface stations with available data from Schmale et al (2016) (black symbols). Models are TM4-ECPL (in red) and NorESM (in green). Units are cm^{-3} . Dashed lines provide the width of one standard deviation of observations and model results with the respective colors.

Seasonality: Both models capture the CCN seasonality (Figure 7) at most stations but Cabauw, where both fail to reproduce the spring maximum. A smaller spring maximum is however simulated by TM4-ECPL at Jungfraujoch despite the overprediction of the CCN levels by the model compared to the observations (Figure 10e,f). Such seasonality is not reproduced by NorESM, which however simulated CCN levels closer to observations. These differences in model performance and seasonal behavior are under investigation analyzing also the differences in size-resolved chemical composition of the aerosols and the natural and anthropogenic emissions used in the models. In particular, the ratio between CCN ($ss=0.5\%$)/CCN ($ss=0.2\%$) is an indicator for the size distribution in the model and the observations. According to these preliminary results, TM4-ECPL seems to overestimate the presence of fine aerosol leading to higher ratios than observed, while the NorESM overestimate is very small.

Furthermore, analysis of these results is ongoing in order to evaluate the importance of various aerosol components, size distribution and hygroscopicity values in the differences between models and observations.

2. Parameterizations of INP as a function of aerosol components

2.1. INP field experiments

2.1.1. BACCHUS campaign at Mace Head (North East Atlantic)

Ice phase transitions in mixed phase clouds are poorly represented in numerical models (McCoy et al., 2015), leading to uncertainties associated with cloud phase (liquid/ice) partitioning, cloud precipitation rates and atmospheric radiative transfer. Atmospheric ice nucleating particles (INPs) play an important role within these complex aerosol-cloud-climate interactions, enabling heterogeneous ice formation. Sea spray aerosol, particles generated from wave breaking and bubble bursting, is a weak INP source in comparison to terrestrial sources (DeMott et al., 2016). However, it has been hypothesized (Schnell and Vali, 1976) and demonstrated (Burrows et al., 2013, Wilson et al., 2015; McCluskey et al., 2016) that marine organic aerosol arising from oceanic biological activity serves as a potentially important source of marine INPs to the high latitude marine boundary layer and clouds forming over it.

The Mace Head Observatory (MHO) is located on the west coast of Ireland (53.32 °N, 9.90 °W) and has been utilized as a natural laboratory for pristine marine aerosol research for over 50 years. Marine organic aerosol plumes, or periods of high marine organic aerosol concentrations associated with elevated offshore biological activity, are often observed at MHO (O'Dowd et al., 2004). This location provides access to ambient pristine marine air, yet the composition and abundance of marine INPs has not been investigated at MHO.

In August 2015, two aerosol filters were collected daily at the top of the 10 meter mast; total sample collection periods ranged from 6 - 37 hrs (20 hrs on average). The pump for the “clean sector filter” was powered using the MHO Clean Sector Sampler (Rinaldi et al., 2009), which collects particles only when black carbon < 15 ng/m³ and wind direction is between 190 to 300 degrees. The pump for the “all sector filter” was powered continuously during the total collection period. The clean sector filters represent aerosol from pristine marine air and the all sector filters represent aerosol from both marine and terrestrial sources. Particles on filters were suspended in pure water for analysis using an ice spectrometer (DeMott et al., 2016), providing INP number concentrations n_{INP} as a function of temperature. Additionally, an offline heating test was performed on a portion of the collected aerosol suspension (heating to 98 °C for 20 mins) to determine the contribution of biological INPs within the different sectors. Future tests, including size filtering and hydrogen peroxide digestions (treatment to determine the role of organic carbon), will be completed.

Total number concentrations of INPs active at $-15\text{ }^{\circ}\text{C}$ ($n_{\text{INP},-15\text{ }^{\circ}\text{C}}$), shown in Figure 11, ranged from 0.0005 to 0.009 L^{-1} . Highest $n_{\text{INP},-15\text{ }^{\circ}\text{C}}$ were often associated with elevated organics and two specific events indicate important contributions of marine and terrestrial organic aerosol to the total INP population at MHO.

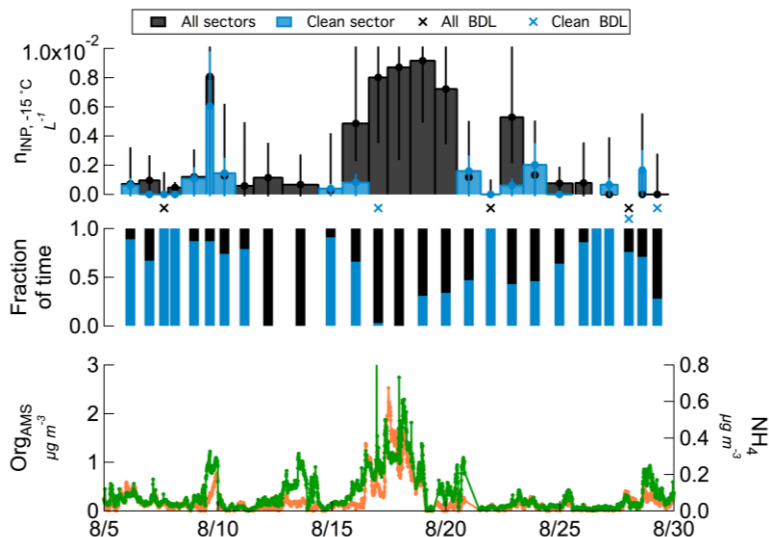


Figure 11. Timelines of (Top) INP number concentrations active at $-15\text{ }^{\circ}\text{C}$, (Middle) fraction of time spent in clean sector, (Bottom) organic aerosol mass concentrations at the MHO. Crosses indicate samples that were below detection limit (BDL).

On 9 August, the dominant air mass for the collection period was pristine marine air and organic aerosol concentrations were elevated ($0.92 \pm 0.1\text{ }\mu\text{g m}^{-3}$) compared to the surrounding days ($<0.3\text{ }\mu\text{g m}^{-3}$). This sampling period was characteristic of a marine organic plume event and total marine n_{INPs} in the clean and all sector filters increased (a factor of 15 increase in INPs active at $-15\text{ }^{\circ}\text{C}$), providing evidence for marine INP enhancement associated with marine organic aerosol. On 16-20 August, meteorological conditions led to terrestrial-dominated sampling periods and organic and ammonium aerosol mass concentrations reached highest levels observed during the study. During this terrestrial organic event (possibility influenced by agriculture), total n_{INP} increased to maximum values (a factor of 35 increase in INPs active at $-15\text{ }^{\circ}\text{C}$). Heat treatments were performed on select samples and representative n_{INP} temperature spectra are shown in Figure 12 for the most commonly observed set INP spectra (10-11 Aug), for the marine organic aerosol plume event (9 Aug) and for the terrestrial INP event that contained elevated organics and ammonium. During baseline conditions, INPs associated with the marine and terrestrial aerosol are heat-stable and therefore not protein-containing biological particles (i.e., bacteria or microbial). However, heating tests indicate that nearly all INPs measured during the marine organic aerosol plume were biological (heat labile). Heating treatments have not been completed for the terrestrial INP event.

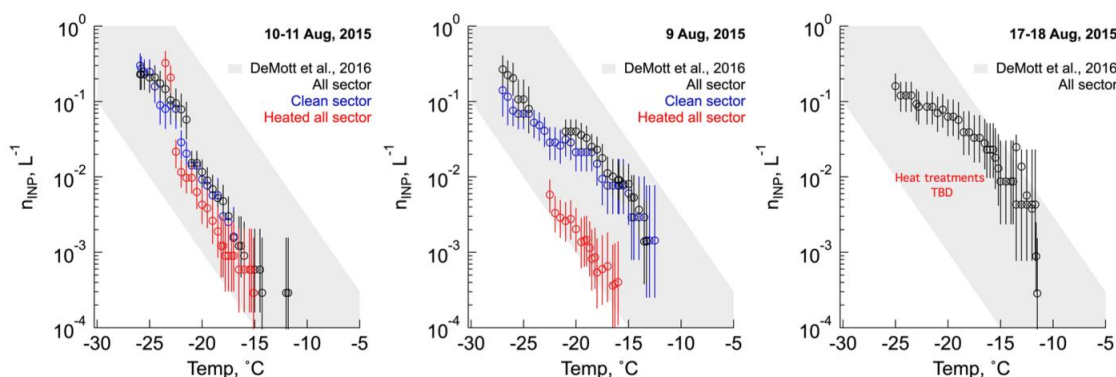


Figure 12. Number concentrations of INPs as a function of temperature for three sampling periods, including the all sector filter (black), clean sector filter (blue) and heat-treated samples (red). (Left) 10-11 August, representative of normal baseline conditions, (Middle) 9 August, representative of the marine organic aerosol plume event and (Right) 17-18 August, representative of the terrestrial aerosol with elevated organics and ammonium. Uncertainty bars correspond to the 95th percent confidence intervals, calculated based on Poisson counting statistics. Estimated boundaries of INP number concentrations reported by DeMott et al., 2016 are shown in the grey shaded area

Another important and impactful finding from these data deals with sampling strategies for studying marine INPs. On 22-23 August, 57% of the sampling time was considered non-clean sector, or terrestrial, and INP spectra indicated significantly more INPs were present on the all sector filter. This comparison reveals an important consideration for measuring marine INPs: terrestrial aerosol can easily contaminate coastal marine samples (Figure 12, left). This apparent terrestrial influence is echoed in other samples, including those collected on 24-25 August (Figure 12, right). Interestingly, the impact of terrestrial aerosol is not consistent, as samples collected with the same percentage of time spent in the terrestrial sector (23-24 August, Figure 13, middle), shows no significant difference between clean and all sector filters.

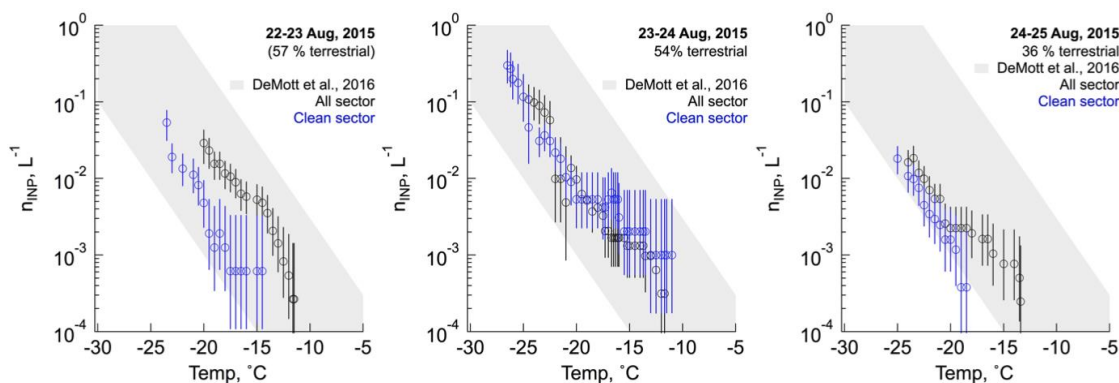


Figure 13. Number concentrations of INPs as a function of temperature for three sampling periods, including the all sector filter (black) and clean sector filter (blue), including (Left) 22-23 August (57% terrestrial), (Middle) 23-24 August (45% terrestrial) and (Right) 24-25 August (36% terrestrial). Uncertainty bars correspond to the 95th percent confidence intervals, calculated based on Poisson counting statistics. Estimated boundaries of INP number concentrations reported by DeMott et al., 2016 are shown in the grey shaded area

From these data, we conclude that future studies at coastal sites aimed towards quantifying ambient marine INP number concentrations should utilize a system similar to the clean sector sampler to isolate the marine INP signal from non-marine INPs.

2.2. INP laboratory experiments

The ice nucleation ability in the immersion mode of 15 natural desert dust samples was investigated (Boose et al., 2016). Four samples had been collected airborne or deposition after atmospheric transport, were measured with the Immersion Mode Cooling Chamber, IMCA (Lüönd et al., 2010) between 236 and 249 K. Additionally, particles of four dust samples were collected on filters for subsequent offline analysis with the Frankfurt Ice Deposition Freezing Experiment (FRIDGE) counter operated in the droplet freezing mode as described by Ardon-Dryer and Levin (2014) and Hiranuma et al. (2015). The ice nucleation ability was quantified by the frozen fraction (FF) and ice-active surface site density (n_s), and compared with the bulk dust mineralogy. A diverse mineralogical composition was found for the different desert dust samples which can be related to variable ice nucleation abilities.

An overview of the n_s of the different desert dust samples is given in Fig. 14. The average $n_s(T)$ of all measured curves was fitted by using

$$n_s = \exp(-a(T - 273.15 \text{ K}) + b)$$

with the fit parameters $a = 0.33 \text{ K}^{-1}$ and $b = 15.64$ and is shown as a black line.

Overall the Australian sample is by far the most ice nucleation-active sample. The Israel milled, the Great Basin, and the Peloponnese sample show a low ice nucleation activity. Generally, the airborne samples, which all originated from the Sahara, are in the lower half of the ice nucleation activity, i.e. less ice-active than most surface-collected samples. This is related to the different mineralogy of the dust samples. While the airborne Saharan samples contain a high fraction of clay minerals, which have a comparably low ice nucleation activity, some of the ground-collected samples from other deserts contain a large fraction of quartz and/or feldspars, which show a higher ice-nucleation activity.

The variation between the different samples in temperature was up to 10 K. To more adequately describe immersion freezing by desert dust in the atmosphere, mineralogy sensitive emission and transport schemes would be desirable. We suggest, K-feldspar for temperatures above 250 K and additionally at lower temperatures Na-plagioclase feldspars and quartz emissions and transport should be quantified. Since this is complex and computationally expensive to implement, more studies quantifying the ice nucleation ability of dust as it is found in the atmosphere may circumvent this complexity.

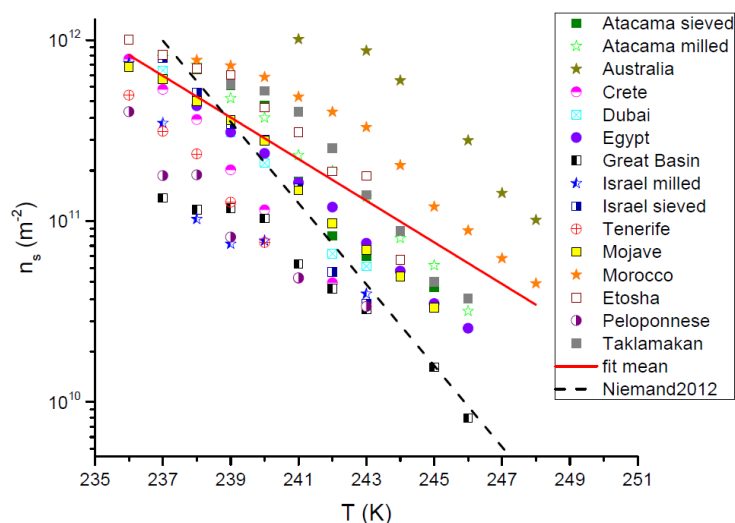


Figure 14. Ice-active surface site density vs. temperature of 15 natural dust samples. Data were binned into 1 K intervals. Squares: surface-collected and sieved, stars: surface-collected and milled and circles: airborne samples.

2.3. Global INP modelling studies

ULEEDS developed a global model of INP concentrations relevant for mixed-phase clouds based on laboratory measurements of ice nucleation by K-feldspar (an ice-active component of desert dust) and marine organic aerosols (from sea spray). The current representation of heterogeneous freezing in operational climate models is usually based on parameterizations that depend on the temperature (Meyers et al., 1992; Young, 1974), or the size distribution of aerosol particles as well as the temperature (DeMott et al., 2010). The results from BACCHUS show that new simulations of the global distribution of INP concentrations based on K-feldspar and sea spray species agree better with ambient measurements than when INP concentrations are assumed to depend only on temperature or particle size.

We used the GLOMAP-mode global aerosol model described in Mann et al. (2010). In our baseline model aerosol mass concentrations for different species, and the particle number concentration are tracked in seven internally mixed log-normal modes (four soluble and three insoluble).

Feldspar is emitted in the model as a fraction of the mass of dust into a separate tracer to the rest of mineral dust. In order to represent the ice nucleating ability of K-feldspar we assume that 35% of the total feldspar is K-feldspar, as assumed in Atkinson et al. (2013), and then we apply the parameterization for the number of active sites (n_s) shown in Atkinson et al. (2013). By using this parameterization we assume that all the different varieties of K-feldspar nucleate ice with the same efficiency.

To represent primary marine organic aerosols in GLOMAP-mode, we developed a parameterization of the organic mass fraction of submicron sea spray particles to fit the observations of water insoluble organic matter (WIOM) at Amsterdam Island (37.48°S, 77.34°E) and Mace Head (53.33°N, 9.9°W). The marine organic component is assumed to be internally mixed with sea-salt. To match the seasonal cycle of WIOM at these two sites, the organic emission parameterisation includes a positive dependence of WIOM mass fraction on chlorophyll (O'Dowd et al., 2015; Rinaldi et al., 2013; Gantt et al., 2011), but a negative dependence on wind speed. Thus, the WIOM is essentially diluted in the sea spray particles when the total sea spray emission flux is high. The parameterization is similar to previous chlorophyll based parameterizations such as Rinaldi et al. (2013); Gantt et al. (2011) but scaled to fit the observations in Amsterdam Island and Mace Head. The values corresponding to the concentrations in these 2 stations agree with the observations within a factor of 2 (see

Vergara Temprado et al., 2016). To calculate INP concentrations from WIOM we use the parameterization in Wilson et al. (2015).

Simulated INP concentrations at the surface are shown in Figure 15 for an activation temperature of -15°C . These concentrations are equivalent to those that would be measured by an INP instrument set to measure at this temperature. Feldspar dominates the INP concentration in environments influenced by terrestrial dust emission sources such as the Sahara and the Asian dust belt. However, concentrations fall rapidly with distance away from sources because the large size feldspar-containing dust particles are rapidly removed from the atmosphere. Desert dust emissions are also sporadic in nature, with strong day-to-day and seasonal variability. The concentrations of INP from K-feldspar and marine organics are summarized in Figure 15c and comparison with panels 15a and 15b reveals that INP from deserts far outnumber INP from sea spray throughout much of the low and mid-latitudes, which are strongly influenced by desert dust, but marine organics become more important in the world's remote oceans.

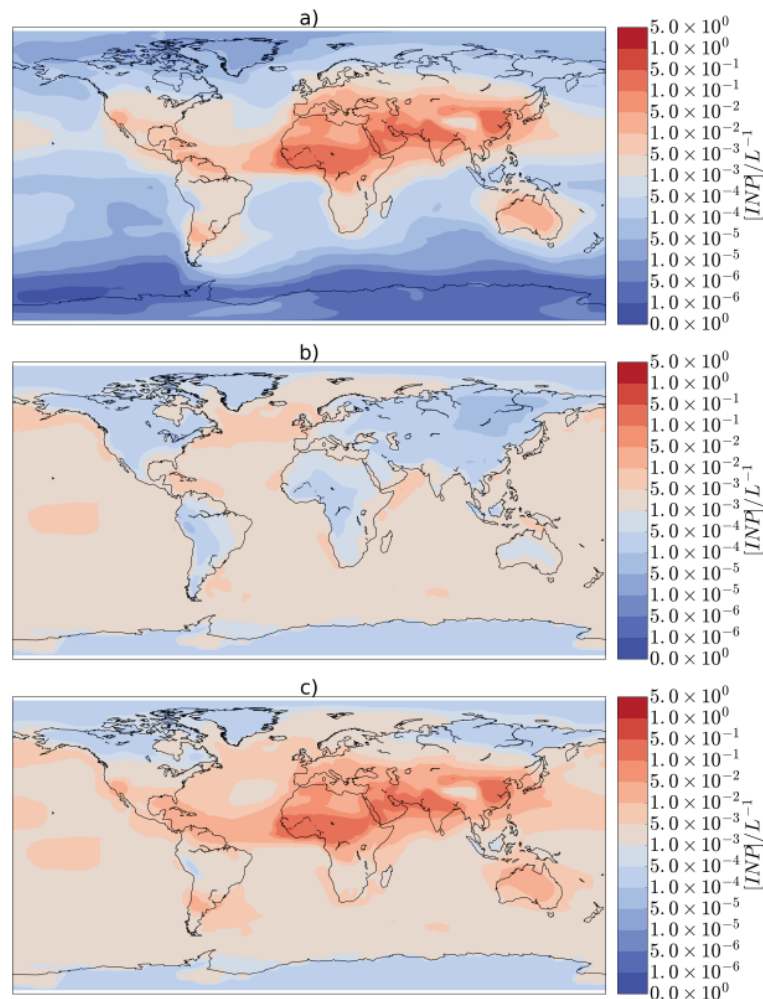


Figure 15. Yearly mean distributions of ice nucleating particles concentrations, for an activation temperature of -15°C . Based on (a) feldspar and (b) marine organics. (c) Total INP concentration obtained by summing the INP concentrations from K-feldspar and marine organics.

Figure 16 shows the $[\text{INP}]_{\text{ambient}}$ concentration (i.e., at ambient temperature) of marine organics and K-feldspar for the different seasons of the year. Feldspar dominates $[\text{INP}]_{\text{ambient}}$ on a 3-monthly mean basis across the northern hemisphere, while marine organic aerosols tend to be important in southern high latitudes, such as those corresponding to the Southern Ocean and Antarctica (Figure 17).

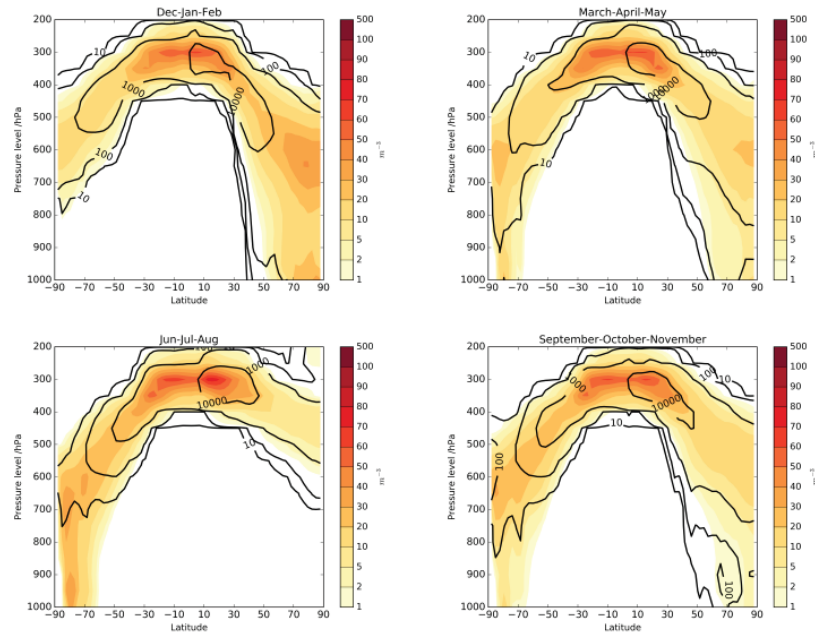


Figure 16. Zonal mean profiles of $[\text{INP}]_{\text{ambient}}$ for every month of the year. The black contour lines correspond to the INP concentration of K-feldspar aerosols (m^{-3}), while the color map shows the INP concentration of marine organic aerosol. The values correspond to 3-monthly mean values calculated using daily concentrations and temperatures.

Figure 17 shows the percentage of days per season when the concentration of $[\text{INP}]_{\text{ambient}}$ from marine organics is greater than the concentration from K-feldspar. We calculate this frequency because high dust concentrations are often associated with episodic dust plumes, so the seasonal mean INP may not reflect the relative contributions of desert dust and sea spray INPs on a day-to-day basis. Overall, over the northern hemisphere, marine organic INP concentrations are greater than K-feldspar INP concentrations between 10% and 30% of the days when the temperature is within the mixed-phase range and the total concentration of $[\text{INP}]_{\text{ambient}}$ is larger than 10^{-4} L^{-1} . It is striking that the contribution of marine organics is more important than K-feldspar on a significant fraction of days in the Northern Hemisphere because in these zonal mean plots we are averaging across the Eurasian and North American continents where the influence of marine organics is minor. In fact, Figure 17 suggests that marine organics are more important than K-feldspar in the North Atlantic, for example, on 10-40 % of days at 600 hPa. In the Southern Hemisphere, the importance of marine organic aerosols is more consistent. Both on a monthly mean basis and on the large majority of days, marine organic aerosols are dominant for INP from March through to November. On the other hand, K-feldspar cannot always be ruled out as an important source of INP in the southern high latitudes in the period from March to November, since there are still several days per month (10 to 60%) when the concentration of transported K-feldspar INP, particularly from South American and Australian sources, dominates over marine organics. Conversely, during December to February at southern high latitudes, K-feldspar mineral dust is more important on more days than marine organic aerosols (Fig. 17a). This is related to higher dust concentrations during the austral summer.

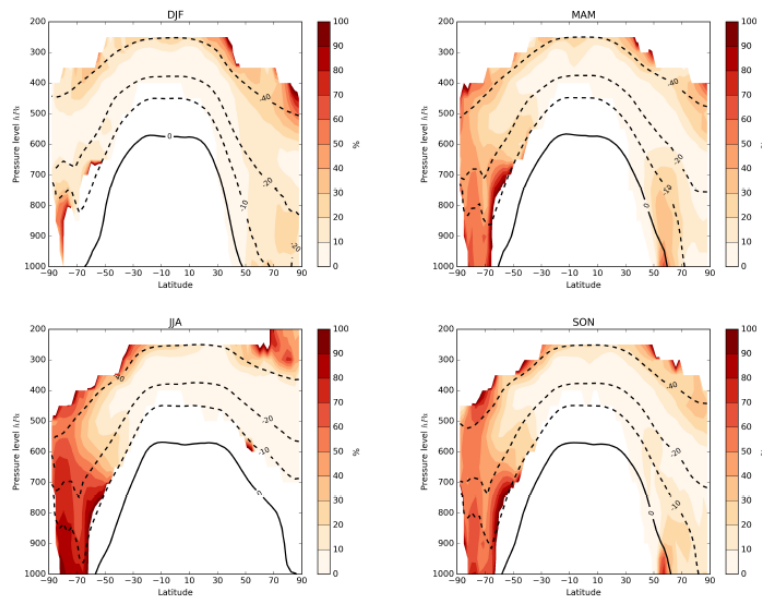


Figure 17. Fraction of days per season when $[INP]_{\text{ambient}}$ from marine organic aerosols is greater than from K-feldspar. The number of days was calculated only for times and locations where the total $[INP]_{\text{ambient}}$ concentration is larger than 0.1 m^{-3} . The black contour lines represent the isothermal lines.

In Figure 18 we compare several singular INP parameterisations with observations. The scheme of Meyers et al. (1992), which relates $[INP]_{\text{T}}$ to temperature and is independent of aerosol properties, is clearly a poor representation of many INP measurements in the atmosphere (Table 3). The DeMott et al. (2010) parameterisation, in which $[INP]_{\text{T}}$ is predicted on the basis of the concentration of particles larger than $0.5 \mu\text{m}$ and temperature has a similar performance to Meyers et al. (1992) as it still tends to overpredict $[INP]_{\text{T}}$, although scaling of the predicted values by multiplying them with 10 a factor to fit the observations might greatly improve its performance as it has a better correlation coefficient (Table 3). It should be borne in mind that DeMott et al. (2010) state that they would expect their parameterisation to overpredict in regions with significant amounts of sea spray aerosol. We also note that in our analysis we use particle concentrations from our model, whereas DeMott et al. (2010) used aerosol measurements coincident with their INP measurements and obtained a better representation of the $[INP]_{\text{T}}$ data.

Table 3. Statistical performance of the different parameterizations of global INP. Pt1 and Pt1.5 are the percentages of data points reproduced within an order of magnitude and 1.5 orders of magnitude. The correlation coefficient has been calculated with the logarithm of the values.

Parameterization	Temperature range/ $^{\circ}\text{C}$	Measurement data points	Pt1	Pt1.5	R(log)
Meyers et al. (1992)	0 to -37	479	35.5%	51%	0.57
DeMott et al. (2010)	0 to -37	479	17%	27.5%	0.686
Niemand et al.(2012)	-12 to -33	438	33.7%	53%	0.58
Marine + K-feldspar	-6 to -25	354	56.7%	74%	0.625

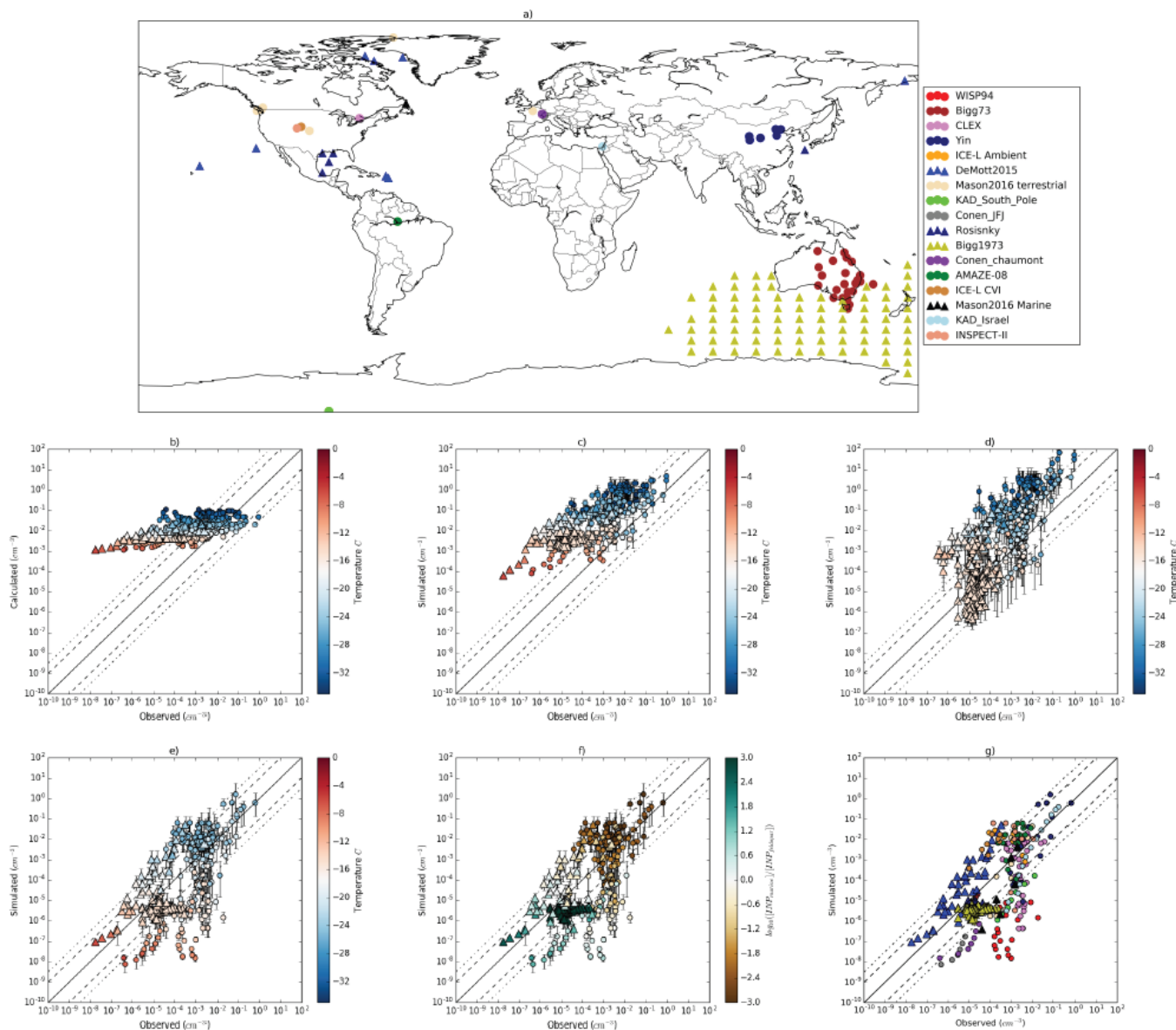


Figure 18. Evaluation of the GLOMAP global INP model against observations. a) Location of the data used for model evaluation. (a-g) Modeled INP concentration values when using: b) Meyers parameterization (Meyers et al., 1992); c) DeMott's parameterization (DeMott et al., 2010) combined with a global aerosol simulation using GLOMAP-mode; d) Niemand dust parameterization (Niemand et al., 2012); e) Our two-species representation based on feldspar (Atkinson et al., 2013) and marine organic aerosols (Wilson et al., 2015). f) Same as e) but showing the relative contribution (in orders of magnitude) of every aerosol species to the simulated concentration. g) Same as e) but showing the data split by the different campaigns shown in a)(with the same colors). Triangles represent marine influenced regions and points terrestrial environments. The dashed lines represent one order of magnitude of difference between modelled and observed and the dashed-dotted lines 1.5 orders of magnitude. The simulated values correspond to an annual mean concentration and the error bars correspond to the simulated seasonality of INP calculated with monthly mean values. For Niemand's dust parameterization (Niemand et al., 2012) the range of data is within the range of temperatures shown in Niemand et al. (2012) (-12 to -33°C).

Using the Niemand et al. (2012) parameterization of dust (with no additional marine organic INP) overestimates many observations by a factor 100-1000 in marine regions (triangles). This overprediction is in part caused by the assumption that all kinds of dust particles nucleate ice with the same efficiency. With this

approach, the smallest dust particles are transported long distances. However, feldspars exist mainly in the large dust particles (silt fraction) so they are not transported as efficiently to remote locations.

Finally, we compare our two-species representation of INP with the same $[\text{INP}]_T$ dataset (Figures 18e-g). The observations used in this comparison are within the range of temperatures of the parameterizations (-5 to -27°C). In this case our representation of INP (Fig 18e) is able to reproduce 56.7% of the observations within an order of magnitude and 74% within 1.5 orders of magnitude (Table 3). The contributions of K-feldspar and marine organics to the simulated INP concentrations of each data point are illustrated in Figure 18g. Marine organics explain more than 90% of the INP concentrations in marine influenced environments and some terrestrial environments with low concentrations of INP (corresponding to high temperature observations). K-Feldspar, however, explains most of the observations in terrestrial regions. The large biases observed when using non-species dependent parameterizations over marine regions are largely corrected, as most marine influenced INP concentrations are simulated within an order of magnitude (72% of marine points), although, some biases are apparent.

3. Reference list

- Abdul-Razzak, H. and Ghan, S. J.: A parameterization of aerosol activation 2. Multiple aerosol types, *J. Geophys. Res.*, 105, 6837–6844, 2000.
- Andreae, M. O., Acevedo, O. C., Araùjo, A., Artaxo, P., Barbosa, C. G. G., Barbosa, H. M. J., Brito, J., Carbone, S., Chi, X., Cintra, B. B. L., da Silva, N. F., Dias, N. L., Dias-Júnior, C. Q., Ditas, F., Ditz, R., Godoi, A. F. L., Godoi, R. H. M., Heimann, M., Hoffmann, T., Kesselmeier, J., Könemann, T., Krüger, M. L., Lavric, J. V., Manzi, A. O., Lopes, A. P., Martins, D. L., Mikhailov, E. F., Moran-Zuloaga, D., Nelson, B. W., Nölscher, A. C., Santos Nogueira, D., Piedade, M. T. F., Pöhlker, C., Pöschl, U., Quesada, C. A., Rizzo, L. V., Ro, C. U., Ruckteschler, N., Sá, L. D. A., de Oliveira Sá, M., Sales, C. B., dos Santos, R. M. N., Saturno, J., Schöngart, J., Sörgel, M., de Souza, C. M., de Souza, R. A. F., Su, H., Targhetta, N., Tóta, J., Trebs, I., Trumbore, S., van Eijck, A., Walter, D., Wang, Z., Weber, B., Williams, J., Winderlich, J., Wittmann, F., Wolff, S., and Yáñez-Serrano, A. M.: The Amazon Tall Tower Observatory (ATTO): overview of pilot measurements on ecosystem ecology, meteorology, trace gases, and aerosols, *Atmos. Chem. Phys.*, 15, 10723-10776, 2015.
- Ardon-Dryer K. and Levin Z., Ground-based measurements of immersion freezing in the eastern Mediterranean - *Atmospheric Chemistry and Physics*, 10, 5217-5231, 2014.
- Bougiatioti, A., Stavroulas, I., Kostenidou, E., Zarnpas, P., Theodosi, C., Kouvarakis, G., Canonaco, F., Prévôt, A. S. H., Nenes, A., Pandis, S. N., and Mihalopoulos, N.: Processing of biomass-burning aerosol in the eastern Mediterranean during summertime, *Atmos. Chem. Phys.*, 14, 4793-4807, 2014
- Burrows, S. M., C. Hoose, U. Pöschl, and M. G. Lawrence, 2013: Ice nuclei in marine air: biogenic particles or dust? *Atmospheric Chemistry and Physics*, 13, 245–267, doi:10.5194/acp-13-245-2013.
- Chang, R. Y. W., Slowik, J. G., Shantz, N. C., Vlasenko, A., Liggio, J., Sjostedt, S. J., Leaitch, W. R., and Abbatt, J. P. D.: The hygroscopicity parameter (κ) of ambient organic aerosol at a field site subject to biogenic and anthropogenic influences: relationship to degree of aerosol oxidation, *Atmos. Chem. Phys.*, 10, 5047-5064, 2010.
- Daskalakis, N., Myriokefalitakis, S., and Kanakidou, M.: Sensitivity of tropospheric loads and lifetimes of short lived pollutants to fire emissions, *Atmos. Chem. Phys.*, 15, 3543-3563, doi:10.5194/acp-15-3543-2015, 2015
- DeCarlo, P. F., Kimmel, J. R., Trimborn, A., Northway, M. J., Jayne, J. T., Aiken, A. C., Gonin, M., Fuhrer, K., Horvath, T., Docherty, K. S., Worsnop, D. R., and Jimenez, J. L.: Field-deployable, high-resolution, time-of-flight aerosol mass spectrometer, *Anal Chem*, 78, 8281-8289, DOI:10.1021/Ac061249n, 2006.
- DeMott, P. J., Prenni, a. J., Liu, X., Kreidenweis, S. M., Petters, M. D., Twohy, C. H., Richardson, M. S., Eidhammer, T., and Rogers, D. C.: Predicting global atmospheric ice nuclei distributions and their impacts on climate., *Proceedings of the National Academy of Sciences of the United States of America*, 107, 11 217–11 222, doi:10.1073/pnas.0910818107,
- DeMott, P. J., and Coauthors, 2016: Sea spray aerosol as a unique source of ice nucleating particles. *Proceedings of the National Academy of Sciences*, 113, 5797–5803.
- Dusek, U., Frank, G. P., Curtius, J., Drewnick, F., Schneider, J., Kürten, A., Rose, D., Andreae, M. O., Borrmann, S., and Pöschl, U.: Enhanced organic mass fraction and decreased hygroscopicity of cloud condensation nuclei (CCN) during new particle formation events, *Geophysical Research Letters*, 37, n/a-n/a, 2010.

- Gantt, B., Meskhidze, N., Facchini, M. C., Rinaldi, M., Ceburnis, D., and O'Dowd, C. D.: Wind speed dependent size-resolved parameterization for the organic mass fraction of sea spray aerosol, *Atmospheric Chemistry and Physics*, **11**, 8777–8790, doi:10.5194/acp-11-8777-2011, 2011.
- Gunthe, S. S., King, S. M., Rose, D., Chen, Q., Roldin, P., Farmer, D. K., Jimenez, J. L., Artaxo, P., Andreae, M. O., Martin, S. T., and Pöschl, U.: Cloud condensation nuclei in pristine tropical rainforest air of Amazonia: size-resolved measurements and modeling of atmospheric aerosol composition and CCN activity, *Atmos. Chem. Phys.*, **9**, 7551–7575, 2009.
- Gunthe, S. S., Rose, D., Su, H., Garland, R. M., Achtert, P., Nowak, A., Wiedensohler, A., Kuwata, M., Takegawa, N., Kondo, Y., Hu, M., Shao, M., Zhu, T., Andreae, M. O., and Pöschl, U.: Cloud condensation nuclei (CCN) from fresh and aged air pollution in the megacity region of Beijing, *Atmos. Chem. Phys.*, **11**, 11023–11039, 2011.
- Hiranuma, N., Augustin-Bauditz, S., Bingemer, H., Budke, C., Curtius, J., Danielczok, A., Diehl, K., Dreischmeier, K., Ebert, M., Frank, F., Hoffmann, N., Kandler, K., Kiselev, A., Koop, T., Leisner, T., Möhler, O., Nillius, B., Peckhaus, A., Rose, D., Weinbruch, S., Wex, H., Boose, Y., DeMott, P. J., Hader, J. D., Hill, T. C. J., Kanji, Z. A., Kulkarni, G., Levin, E. J. T., McCluskey, C. S., Murakami, M., Murray, B. J., Niedermeier, D., Petters, M. D., O'Sullivan, D., Saito, A., Schill, G. P., Tajiri, T., Tolbert, M. A., Welti, A., Whale, T. F., Wright, T. P., and Yamashita, K.: A comprehensive laboratory study on the immersion freezing behavior of illite NX particles: a comparison of 17 ice nucleation measurement techniques, *Atmos. Chem. Phys.*, **15**, 2489–2518, doi:10.5194/acp-15-2489-2015, 2015.
- Hitzenberger, R., Giebl, H., Petzold, A., Gysel, M., Nyeki, S., Weingartner, E., Baltensperger, U., and Wilson, C. W.: Properties of jet engine combustion particles during the PartEmis experiment. Hygroscopic growth at supersaturated conditions, *Geophysical Research Letters*, **30**, n/a-n/a, 2003.
- Hyvärinen, A. P., Kolmonen, P., Kerminen, V. M., Virkkula, A., Leskinen, A., Komppula, M., Hatakka, J., Burkhardt, J., Stohl, A., Aalto, P., Kulmala, M., Lehtinen, K. E. J., Viisanen, Y., and Lihavainen, H.: Aerosol black carbon at five background measurement sites over Finland, a gateway to the Arctic, *Atmos. Environ.*, **45**, 4042–4050, 2011.
- Jimenez, J. L., Canagaratna, M. R., Donahue, N. M., Prevot, A. S. H., Zhang, Q., Kroll, J. H., DeCarlo, P. F., Allan, J. D., Coe, H., Ng, N. L., Aiken, A. C., Docherty, K. S., Ulbrich, I. M., Grieshop, A. P., Robinson, A. L., Duplissy, J., Smith, J. D., Wilson, K. R., Lanz, V. A., Hueglin, C., Sun, Y. L., Tian, J., Laaksonen, A., Raatikainen, T., Rautiainen, J., Vaattovaara, P., Ehn, M., Kulmala, M., Tomlinson, J. M., Collins, D. R., Cubison, M. J., E., Dunlea, J., Huffman, J. A., Onasch, T. B., Alfarra, M. R., Williams, P. I., Bower, K., Kondo, Y., Schneider, J., Drewnick, F., Borrmann, S., Weimer, S., Demerjian, K., Salcedo, D., Cottrell, L., Griffin, R., Takami, A., Miyoshi, T., Hatakeyama, S., Shimono, A., Sun, J. Y., Zhang, Y. M., Dzepina, K., Kimmel, J. R., Sueper, D., Jayne, J. T., Herndon, S. C., Trimborn, A. M., Williams, L. R., Wood, E. C., Middlebrook, A. M., Kolb, C. E., Baltensperger, U., and Worsnop, D. R.: Evolution of Organic Aerosols in the Atmosphere, *Science*, **326**, 1525–1529, doi:10.1126/science.1180353, 2009
- Juranyi, Z., Gysel, M., Duplissy, J., Weingartner, E., Tritscher, T., Dommen, J., Henning, S., Ziese, M., Kiselev, A., Stratmann, F., George, I., and Baltensperger, U.: Influence of gas-to-particle partitioning on the hygroscopic and droplet activation behaviour of [small alpha]-pinene secondary organic aerosol, *Phys. Chem. Chem. Phys.*, **11**, 8091–8097, 2009.
- Jurányi, Z., Gysel, M., Weingartner, E., DeCarlo, P. F., Kammermann, L., and Baltensperger, U.: Measured and modelled cloud condensation nuclei number concentration at the high alpine site Jungfraujoch, *Atmos. Chem. Phys.*, **10**, 7891–7906, 2010.
- Kirkevåg, A., Iversen, T., Seland, Ø., Hoose, C., Kristjánsson, J. E., Struthers, H., Ekman, A. M. L., Ghan, S., Griesfeller, J., Nilsson, E. D., and Schulz, M.: Aerosol–climate interactions in the Norwegian Earth System Model – NorESM1-M, *Geosci. Model Dev.*, **6**, 207–244, doi:10.5194/gmd-6-207-2013, 2013.
- Lohmann and Diehl Sensitivity Studies of the Importance of Dust Ice Nuclei for the Indirect Aerosol Effect on Stratiform Mixed-Phase Clouds, *Journal of the Atmospheric Sciences* **63**(3) DOI: 10.1175/JAS3662.1, 2006.
- Lohmann, U., Stier, P., Hoose, C., Ferrachat, S., Kloster, S., Roeckner, E., and Zhang, J.: Cloud microphysics and aerosol indirect effects in the global climate model ECHAM5-HAM, *Atmos. Chem. Phys.*, **7**, 3425–3446, doi:10.5194/acp-7-3425-2007, 2007.
- Lohmann, U and C. Hoose, Sensitivity studies of different aerosol indirect effects in mixed-phase clouds, *Atmos. Chem. Phys.*, **9**, 8917–8934, 2009.
- Lüönd, F., O. Stetzer, A. Welti, and U. Lohmann (2010), Experimental study on the ice nucleation ability of size-selected kaolinite particles in the immersion mode, *J. Geophys. Res.*, **115**, D14201, doi:10.1029/2009JD012959.
- Makkonen, R., Seland, Ø., Kirkevåg, A., Iversen, T., and Kristjánsson, J. E.: Evaluation of aerosol number concentrations in NorESM with improved nucleation parameterization, *Atmos. Chem. Phys.*, **14**, 5127–5152, doi:10.5194/acp-14-5127-2014, 2014.

- Mann, G. W., Carslaw, K. S., Spracklen, D. V., Ridley, D. a., Manktelow, P. T., Chipperfield, M. P., Pickering, S. J., and Johnson, C. E.: Description and evaluation of GLOMAP-mode: a modal global aerosol microphysics model for the UKCA composition-climate model, *Geoscientific Model Development*, 3, 519–551, doi:10.5194/gmd-3-519-2010, <http://www.geosci-model-dev.net/3/519/2010/>, 2010.
- Massoli, P., Lambe, A. T., Ahern, A. T., Williams, L. R., Ehn, M., Mikkilä, J., Canagaratna, M. R., Brune, W. H., Onasch, T. B., Jayne, J. T., Petäjä, T., Kulmala, M., Laaksonen, A., Kolb, C. E., Davidovits, P., and Worsnop, D. R.: Relationship between aerosol oxidation level and hygroscopic properties of laboratory generated secondary organic aerosol (SOA) particles, *Geophysical Research Letters*, 37, n/a-n/a, 2010.
- McCluskey, C. S., and Coauthors, 2016: A dynamic link between ice nucleating particles released in nascent sea spray aerosol and oceanic biological activity during two mesocosm experiments, *J. Atmos. Sci.*, doi:10.1175/JAS-D-16-0087.1.
- McCoy, D. T., S. M. Burrows, R. Wood, D. P. Grosvenor, S. M. Elliott, P.-L. Ma, P. J. Rasch, and D. L. Hartmann, 2015: Natural aerosols explain seasonal and spatial patterns of Southern Ocean cloud albedo. *Science Advances*, 1, e1500157–e1500157, doi:10.1126/sciadv.1500157.
- Meyers, M. P., DeMott, P. J., and Cotton, W. R.: New Primary Ice-Nucleation Parameterizations in an Explicit Cloud Model, *Journal of Applied Meteorology*, 31, 708–721, doi:10.1175/1520-0450 (1992).
- Niemand, M., Möhler, O., Vogel, B., Vogel, H., Hoose, C., Connolly, P., Klein, H., Bingemer, H., DeMott, P., Skrotzki, J., and Leisner, T.: A Particle-Surface-Area-Based Parameterization of Immersion Freezing on Desert Dust Particles, *Journal of the Atmospheric Sciences*, 69, 3077–3092, doi:10.1175/JAS-D-11-0249.1, <http://journals.ametsoc.org/doi/abs/10.1175/JAS-D-11-0249.1>, 2012.
- O'Dowd, C., and Coauthors, 2015: Connecting marine productivity to sea-spray via nanoscale biological processes: Phytoplankton Dance or Death Disco? *Scientific Reports*, 5, 14883, doi:10.1038/srep14883.
- O'Dowd, C. D., Facchini, M. C., Cavalli, F., Ceburnis, D., Mircea, M., Decesari, S., Fuzzi, S., Yoon, Y. J., and Putaud, J. P.: Biogenically driven organic contribution to marine aerosol, *Nature*, 431, 676–680, DOI:10.1038/Nature02959, 2004.
- O'Dowd, C., Ceburnis, D., Ovadnevaite, J., Bialek, J., Stengel, D. B., Zacharias, M., Nitschke, U., Connan, S., Rinaldi, M., Fuzzi, S., Decesari, S., Cristina Facchini, M., Marullo, S., Santolero, R., Dell'Anno, A., Corinaldesi, C., Tangherlini, M., and Danovaro, R.: Connecting marine productivity to sea-spray via nanoscale biological processes: Phytoplankton Dance or Death Disco?, *Scientific Reports*, 5, 14883, 10.1038/srep14883, 2015.
- Ovadnevaite, J., Ceburnis, D., Martucci, G., Bialek, J., Monahan, C., Rinaldi, M., Facchini, M. C., Berresheim, H., Worsnop, D. R., and O'Dowd, C.: Primary marine organic aerosol: A dichotomy of low hygroscopicity and high CCN activity, *Geophys Res Lett*, 38, DOI:10.1029/2011gl048869, 2011.
- Petters, M. D. and Kreidenweis, S. M.: A single parameter representation of hygroscopic growth and cloud condensation nucleus activity, *Atmos. Chem. Phys.*, 7, 1961–1971, 2007
- Rinaldi, M., and Coauthors, 2009: On the representativeness of coastal aerosol studies to open ocean studies: Mace Head—a case study. *Atmospheric Chemistry and Physics*, 9, 9635–9646.
- Rinaldi, M., Fuzzi, S., Decesari, S., Marullo, S., Santolero, R., Provenzale, A., von Hardenberg, J., Ceburnis, D., Vaishya, A., O'Dowd, C. D., and Facchini, M. C.: Is chlorophyll- a the best surrogate for organic matter enrichment in submicron primary marine aerosol?, *Journal of Geophysical Research: Atmospheres*, 118, 4964–4973, doi:10.1002/jgrd.50417, <http://doi.wiley.com/10.1002/jgrd.50417>, 2013.
- Rose, D., Gunthe, S. S., Su, H., Garland, R. M., Yang, H., Berghof, M., Cheng, Y. F., Wehner, B., Achtert, P., Nowak, A., Wiedensohler, A., Takegawa, N., Kondo, Y., Hu, M., Zhang, Y., Andreae, M. O., and Pöschl, U.: Cloud condensation nuclei in polluted air and biomass burning smoke near the mega-city Guangzhou, China – Part 2: Size-resolved aerosol chemical composition, diurnal cycles, and externally mixed weakly CCN-active soot particles, *Atmos. Chem. Phys.*, 11, 2817–2836, 2011.
- Rose, D., Nowak, A., Achtert, P., Wiedensohler, A., Hu, M., Shao, M., Zhang, Y., Andreae, M. O., and Pöschl, U.: Cloud condensation nuclei in polluted air and biomass burning smoke near the mega-city Guangzhou, China – Part 1: Size-resolved measurements and implications for the modeling of aerosol particle hygroscopicity and CCN activity, *Atmos. Chem. Phys.*, 10, 3365–3383, 2010.
- Schnell, R. C., and Vali, G. (1974), Freezing nuclei in marine waters. *Tellus*, 27, 321–323. doi:10.1111/j.2153-3490.1975.tb01682.x
- Spracklen, D. V., Carslaw, K. S., Pöschl, U., Rap, A., and Forster, P. M.: Global cloud condensation nuclei influenced by carbonaceous combustion aerosol, *Atmos. Chem. Phys.*, 11, 9067–9087, 2011.
- Stevens, B., et al.: Atmospheric component of the MPI-M Earth System Model: ECHAM6, *J. Adv. Model. Earth Syst.*, 5, 146–172, doi:10.1002/jame.20015, 2013

- Stein, A.F., Draxler, R.R., Rolph, G.D., Stunder, B.J.B., Cohen, M.D., and Ngan, F., (2015). NOAA's HYSPLIT atmospheric transport and dispersion modeling system, *Bull. Amer. Meteor. Soc.*, 96, 2059-2077, <http://dx.doi.org/10.1175/BAMS-D-14-00110.1>
- Stier, P.: Limitations of passive remote sensing to constrain global cloud condensation nuclei, *Atmos. Chem. Phys.*, 16, 6595-6607, doi:10.5194/acp-16-6595-2016, 2016
- Tritscher, T., Dommen, J., DeCarlo, P. F., Gysel, M., Barmet, P. B., Praplan, A. P., Weingartner, E., Prévôt, A. S. H., Riipinen, I., Donahue, N. M., and Baltensperger, U.: Volatility and hygroscopicity of aging secondary organic aerosol in a smog chamber, *Atmos. Chem. Phys.*, 11, 11477-11496, doi:10.5194/acp-11-11477-2011, 2011.
- Vergara Temprado, J., T. W. Wilson, D. O'Sullivan, J. Browse, K. J. Pringle, K. Ardon-Dryer, A. K. Bertram, S. M. Burrows, D. Ceburnis, P. J. DeMott, R. H. Mason, C. D. O'Dowd, M. Rinaldi, B. J. Murray, and K. S. Carslaw: Contribution of feldspar and marine organic aerosols to global ice nucleating particle concentrations, *Atmos. Chem. Phys. Discuss.*, doi:10.5194/acp-2016-822 (2016).
- Vignati, E., J. Wilson, and P. Stier (2004), M7: An efficient size-resolved aerosol microphysics module for large-scale aerosol transport models, *J. Geophys. Res.*, 109, D22202, doi:10.1029/2003JD004485.
- Wang, Y., Liu, X., Hoose, C., and Wang, B.: Different contact angle distributions for heterogeneous ice nucleation in the Community Atmospheric Model version 5, *Atmos. Chem. Phys.*, 14, 10411-10430, doi:10.5194/acp-14-10411-2014, 2014.
- Wilson, T. W., and Coauthors, 2015: A marine biogenic source of atmospheric ice-nucleating particles. *Nature*, 525, 234–238, doi:10.1038/nature14986.
- Young, K. C.: A Numerical Simulation of Wintertime, Orographic Precipitation: Part I. Description of Model Microphysics and Numerical Techniques, *Journal of the Atmospheric Sciences*, 31, 1735–1748, 1974.
- Zhang, K., O'Donnell, D., Kazil, J., Stier, P., Kinne, S., Lohmann, U., Ferrachat, S., Croft, B., Quaas, J., Wan, H., Rast, S., and Feichter, J.: The global aerosol-climate model ECHAM-HAM, version 2: sensitivity to improvements in process representations, *Atmos. Chem. Phys.*, 12, 8911-8949, doi:10.5194/acp-12-8911-2012, 2012

Changes with respect to the DoW

No changes with respect to DoW

Dissemination and uptake

The tested parameterizations are available for the BACCHUS modeling groups to be implemented in regional and earth system models.

Peer-reviewed publications issued from the project (BACCHUS papers)

Boose, Y., Welti, A., Atkinson, J., Ramelli, F., Danielczok, A., Bingemer, H. G., Plötze, M., Sierau, B., Kanji, Z. A., and Lohmann, U.: Heterogeneous ice nucleation on dust particles sourced from 9 deserts worldwide – Part 1: Immersion freezing, *Atmos. Chem. Phys. Discuss.*, doi:10.5194/acp-2016-438, 2016.

Daskalakis, N., Tsigaridis, K., Myriokefalitakis, S., Fanourgakis, G. S., and Kanakidou, M.: Large gain in air quality compared to an alternative anthropogenic emissions scenario, *Atmos. Chem. Phys.*, 16, 9771-9784, doi:10.5194/acp-16-9771-2016, 2016.

Myriokefalitakis S., Nenes A., Baker A.R., Mihalopoulos N., Kanakidou M.: Bioavailable atmospheric phosphorous supply to the global ocean: a 3-D global modelling study, *Biogeosciences Discuss.*, doi:10.5194/bg-2016-215, 2016 in press in *Biogeosciences*.

Schmale et al. (2016) Collocated observations of cloud condensation nuclei, particle size distributions, and chemical composition, *Scientific Data*, SDATA-16-00241.

Vergara Temprado, J., T. W. Wilson, D. O'Sullivan, J. Browse, K. J. Pringle, K. Ardon-Dryer, A. K. Bertram, S. M. Burrows, D. Ceburnis, P. J. DeMott, R. H. Mason, C. D. O'Dowd, M. Rinaldi, B. J. Murray, and K. S. Carslaw: Contribution of feldspar and marine organic aerosols to global ice nucleating particle concentrations, *Atmos. Chem. Phys. Discuss.*, doi:10.5194/acp-2016-822 (2016).

Presentations at Conferences issued from the project (BACCHUS papers)

Fanourgakis G.S., Myriokefalitakis S., Kanakidou M., Study of the CCN formation as a function of aerosol components, poster presentation at the EGU AS4.5 April 2016

Myriokefalitakis S., Fanourgakis G.S., Kanakidou M., The contribution of bioaerosols to the organic carbon mass of the atmosphere, oral presentation at the EGU AS4.5 April 2016.

Vergara Temprado et al., The Global Distribution of Atmospheric Ice Nucleating Particles, AGU A13B-0315, San Francisco, 2015.

Vergara Temprado et al. Global modelling of ice nucleating particles, Sixth Annual Composition-Climate Interaction Meeting, Cambridge, UK, April 2016

Vergara Temprado et al. Marine organic aerosols and k-feldspar as ice nucleating particles in the atmosphere, International Conference on Clouds and Precipitation, Manchester, July 2016

Vergara Temprado et al. Contribution of Marine organics and Feldspar aerosols to global INP concentrations, Recent Advances in Ice Nucleation Particle Research, Fishguard, UK, October 2016.